Jpn. J. Appl. Phys. Vol. 40 (2001) pp. 7031–7046
Part 1, No. 12, December 2001

Production of Stable Isotopes by Selective Channel Photofission of Pd

Akito TAKAHASHI*, Masayuki OHTA and Tadahiko MIZUNO[1]

Department of Nuclear Engineering, Osaka University, Yamadaoka 2-1, Suita, Osaka 565-0871, Japan
[1]*Department of Quantum Energy Engineering, Hokkaido University, Kita 13 Nishi 8, Kita-ku, Sapporo 060-8628, Japan*

(Received May 30, 2001; accepted for publication September 3, 2001)

A conservative modeling and analysis were attempted to explain the presence of nonradioactive fission-like products with nonnatural isotopic ratios observed in some D_2O/Pd electrolysis experiments. The collective deformation of a Pd nucleus by multiphoton E1 resonance absorption in a dynamic PdD_x lattice was assumed to induce low-energy photofissions via the selective scission channels within the lowest band (11–20 MeV) of channel-dependent fission barriers. Values of channel dependent fission barriers were calculated by using liquid drop model potentials for Pd isotopes. Fission products were analyzed in detail. Major fission products (FPs) are stable isotopes and the isotopic ratios of FP elements are very different from those of natural abundances. The present theoretical results have shown good agreement with the experimental data of Mizuno *et al.* [Denki Kagaku **64** (1996) 1660] and others in terms of Z-distribution, mass distribution and isotopic ratios. Selective channel photofissions with positive Q-values are possible for $A > 90$ nuclei, which may provide us with a clean method for the incineration for the radio isotope (RI) waste of nuclear plants.

KEYWORDS: nuclear reaction in PdD_x, selective channel photofission, stable isotope products

1. Introduction

Anomalous deposits of large amounts of foreign elements on cathode metals (such as Pd, Au and W) during electrolysis of heavy water (and sometimes light water) have been reported recently by Mizuno *et al.*,[1)] Miley and Patterson,[2)] Ohmori *et al.*,[3)] Iwamura *et al.*[4)] and others. The amounts of observed foreign elements (such as Fe, Cr, Ti, Ca, Ni, Cu, Zn and Si) were so large that to consider them as impurity concentrations was not feasible. It is also unusual that isotopic ratios of the detected foreign elements have shown markedly different values[1–4)] from those of natural abundances; for example, the ratio of Fe-58/Fe-57/Fe-56 was observed to be[4)] 14/41/45, compared with the natural abundance ratio of 0.282/2.119/91.754. This anomaly of isotopic ratios was observed for Ti, Cr, Fe, Cu, Zn, Si, Mg and other elements. Since the known isotope separation coefficients in chemical and physical processes are very small, of the order of less than 1 to 2%, these anomalies can only be explained by assuming them to be products of some nuclear reactions. Considering the widely distributed data of atomic numbers and mass numbers of the observed foreign elements, fission reaction is regarded as the a priori candidate. However, another unusual fact concerning the above experiments[1–4)] is that no intense radiations (such as γ-rays and neutrons) have been detected, although one recognizes that fission produces many radio isotopes and radiations. The occurrence of nuclear reactions (including fission) can hardly be imagined in the environment of electrochemical processes.

To achieve fission, a target nucleus (Pd, for example) should be excited to the levels comparable to fission barriers (around 15 MeV for Pd, as we will explain later in this work). Miley and Patterson[2)] suggested the Pd + p or Pd + d process for the excitation, however, the excitation energy of p-absorption to Pd is around 8 MeV and far below the fission barrier ($\sim$15 MeV as the lowest value), hence no fission is possible. As an example, in $^{104}Pd + p \rightarrow {}^{105}Ag^*$, $^{105}Ag^*$ promptly emits γ-rays to go to ^{105}Ag (ground state) which decays with electron capture (EC) with a 4.3 day half-life, emitting 344 keV gamma-rays (65% branching) that can be easily detected. Excitation by neutron absorption (around 8 MeV excited energy) is not sufficiently high to achieve fission either. Of course, a significant number (flux) of neutrons does not exist in this system, because if neutrons existed we could easily detect them freely moving and leaking to the outside of the system. Kozima[5)] assumes an ideal trapping of neutrons in metal (or metal-hydride, MH_x) with intense density levels (10^{10}–10^{15} in flux), but obviously there is no force present to keep the neutrons trapped in MH_x: neutrons can move freely and can collide with all of the existing nuclei in the system and leak out with a large probability. Their reaction rates with existing nuclei are accurately calculated by the proven reactor physics codes. If two nucleons are absorbed, the excited energy can approach the fission barrier. For example, the Pd + d process produces Ag^* ($E_x \sim 11$ MeV), although a very strong Coulomb barrier ($\sim$10 MeV) should be overcome. Deuterons at room temperature (or in a chemical process) cannot have any meaningful tunneling probability through such a high Coulomb barrier, and $E_x \sim 11$ MeV is too low a value to achieve fission. We might consider di-neutrons which can produce larger excitations than $\sim$11 MeV. However, di-neutrons with a meaningful lifetime (more than fs) do not exist since there is no binding force between neutrons. Whenever two neutrons were born at a point by chance, they would separate within 10^{-20}–10^{-22} s, and move in different directions, possibly collide with existing nuclei as independent neutrons, and usually leak from the system. Therefore, fissions of metal cathodes (Pd, for instance) by p, d, n or 2n absorption are not plausible in the electrochemical system.

One possibility may be nuclear excitation by photons. The photonuclear reaction involving the E1 giant resonance is well known in nuclear physics. The E1 giant resonance takes place at $E_r \sim 15$ MeV, which is above (or comparable to) the lowest band of fission barriers of Pd isotopes as shown in this work. Energetic photons (γ-rays) as high as 15 MeV have never been observed in cold fusion (CF) electrolysis (or discharge) experiments. However, low-energy photons (0.1–50 keV)

*Correspondent author. E-mail address: akito@nucl.eng.osaka-u.ac.jp

with high flux might be generated in a dynamic $PdD(H)_x$ lattice, for example, by solid plasma oscillation or by quantum electrodynamics (QED) photons from the virtual compound nuclei (^{6}Li* and ^{8}Be*) of coherent multibody deuteron fusion in PdD_x.[6–8] Iwamura *et al*. have reported[4] continuous X-ray emissions in the 10–100 keV region in their gas-diffusion type D_2O/Pd electrolysis which showed the generation of excess heat and anomalous foreign elements. Fukuoka *et al*. have reported similar continuous X-ray emission in their D_2O/Pd electrolysis experiments.[9] Although the availability of an intense 0.1–50 keV photon source in electrochemical systems is yet to be studied, this work assumes the multiphoton absorption process to generate the nuclear excitation around $E_r \sim 15$ MeV.

Of course, the photofission starts with nonradioactive elements. The low-energy photofission (LEPF) may be induced by multiphoton absorption to a high excited state around $E_x = 15$ MeV due to the collective (dumbbell) deformation of the nuclei which may lead to scissions of selective channels having low fission barriers around $E_r = 15$ MeV. This selective channel fission (SCF) for Pd isotopes can produce mostly stable isotope pairs of fission products (FP), as we observe in this work, and nonnatural isotopic ratios in FP elements. The concept of fission-channel-dependent barrier height based on the liquid drop model is the key to this work. The physical bases of the model assumption are described in §2. Detailed analysis of fission products in mass distribution, Z (atomic number)-distribution, isotopic ratios and possible products of radio isotopes are described for 6 Pd isotopes and Au-197 in §3. Summary and conclusion are given in §4. The results of the present analysis are compared with experimental results of Mizuno *et al*.[1] and Iwamura *et al*.[4] for mass and Z-distributions and isotopic ratios.

2. Model Assumptions

2.1 Possible photon sources

We assume that high flux photons in the 0.1–50 keV region would be generated in metal-hydride lattices under dynamic conditions, or that the same level photon beams were irradiated from outside. If we limit the condition to the so called CF electrolysis experiments, the continuous energy X-ray emission in the 10–100 keV region observed by Iwamura *et al*.[4] and Fukuoka *et al*.[9] may give us some encouraging indications. Under the overloading condition $X > 1$ for PdD_x (H_x), lattice plasma oscillation is thought[10] to be induced. High flux QED photons (possibly in the 10–100 eV region) are virtually emitted and absorbed by plasma. Virtual photon flux may be as large as $\phi_p = 10^{22}$(plasma density) $\times$ 3×10^{10}(photon velocity) $= 3 \times 10^{32}$photons/(cm^2 s). However, nuclear excitation by means of the multiphoton process still appears implausible. The dynamic PdD_x condition may however induce the subsequent coherent fusion of deuterons. If the scenario of coherent multibody deuteron fusion[6–8] is correct, one virtual compound nucleus ^{6}Li* (25.3 MeV: 4−) or ^{8}Be* (47.6 MeV: 3−) can transfer $\sim$1000 QED photons per fusion in the 10–100 keV region for plasma oscillation including Pd atoms. Assuming the lifetimes of ^{6}Li* and ^{8}Be* to be of the order of 10^{-15} s, the equivalent peak flux (converted to macroscopic flux assuming the homogeneous generation of multibody fusion) may be of the order of 10^{50} photons/(cm^2 s), which is sufficiently high to induce multiphoton nuclear excitation of neighboring Pd-nuclei near the generated ^{6}Li* or ^{8}Be*. However, the actual macroscopic photon flux is low due to random events of the ^{6}Li* and ^{8}Be* generation. Assuming that 1 W/cc power is generated by the coherent fusion, a very high photon flux of $\phi_p = 10^{11}$[f/(s cm^3)] $\times$ $10^3 \times 3 \times 10^{10}$(photon velocity) $= 3 \times 10^{24}$ photons/(cm^2 s) would be generated in the PdD_x lattice average. We require random short-pulse (ns to fs width) X-ray bursts with a high peak flux of more than 10^{32} p/(cm^2 s). No experimental trials have been conducted to observe such strong X-ray bursts. We expect that pure physics experiments involving X-ray laser irradiation on Pd (and on nuclei with mass > 100), will clarify the effect.

Although the assumed QED photon peak flux is very high, these relatively low-energy photons may be considerably absorbed by photoelectric absorption, Compton scattering and Rayleigh (elastic) scattering by orbital electrons of K-shell to N-shell of the Pd atom, before reaching the Pd nucleus. This feature is illustrated in Fig. 1. A Pd atom has 46 electrons, 10 of which are in the outermost 4d-shell and may behave as conduction-band (quasi-free) electrons, and the remaining 36 electrons behave as a shielding cloud for QED-photons penetrating to the Pd nucleus at the center. We define the probability of QED photon transmission through the orbital electron cloud as P_q (E_q), where E_q is the QED photon energy.

Next we consider that some QED photons can reach the Pd nucleus to achieve multiphoton-E1 absorption and excite the Pd nucleus to a nuclear level by $\Delta E_x = nE_q$. Examples of nuclear levels of Pd are seen in the most recent data sheets.[11] Some low-lying states (which start around 10–100 keV, for $A > 100$ nuclei, in general) of collective nuclear deformation have relatively long lifetimes, of the order of 1 ps–10 ns (Pd-106 for example), compared with lifetimes of prompt γ-decays with values of $\sim 10^{-15}$ s (fs). We can regard these relatively long-lived levels as isometric states, via which the cascade pumping-up of high excited energy might be possible by the multiphoton E2 and E1 transitions (absorptions) starting from the ground-state level. According to the inversely proportional relationship between lifetime and energy width of an excited level, namely by the Heisenberg principle, we should be able to achieve very fine tuning of photon energy to match the excited level with a long lifetime. This is a difficult task. We consider that an intensely peaked ($> 10^{28}$ p cm^{-2} s^{-1}) and short ($<$ ns) burst of a rather white spectrum (in the 0.01–5 MeV region) of photons may contribute better to the pumping-up process through randomly matched level transitions. We speculate that the absorption of multiple (two or three or more) photons may be realized in this way. This means that we need coherent photonbeams such as those from a X-ray or gamma-ray laser. The hypothesized 10–100 keV QED photons with an ultra intense burst ($<$ fs) of about 1000 photons per fusion, by the coherent multibody deuteron fusion, may be regarded as a type of gamma-ray laser produced in the sub-nm domain, in this respect. We expect that photon (electro-magnetic wave) absorption cross sections for the excited (deformed) nuclei may be considerably enhanced due to the antenna principle, although no cross section data are available for the excited nuclei. Level data for excited states as high as 20–15 MeV are also not available[11] at present, and thus the pumping-up pro-

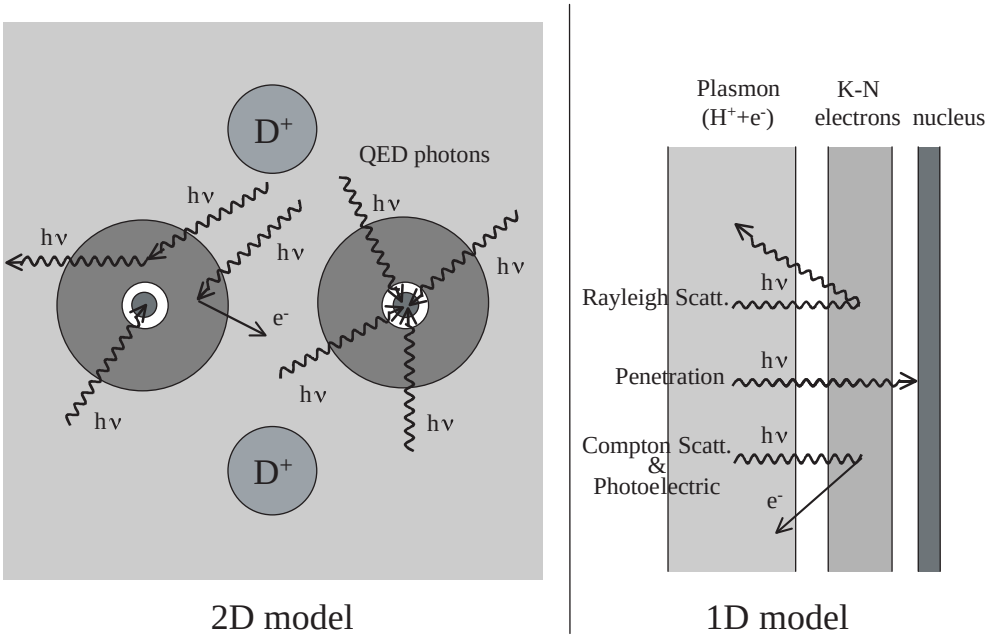

Fig. 1. Multiphoton absorption in Pd nucleus by QED coupling to PdD_x plasma oscillation.

cess to $E_r \sim 15$ MeV remains a crude assumption which can be given by

$$E_x = \sum_{i=1}^{I} \Delta E_{xi}; \quad \Delta E_x = nE_q. \tag{1}$$

To realize selective channel photofission (SCPF), we must assume the excitation condition of $E_x \sim E_r \sim 15$ MeV.

2.2 E1 giant resonance and fission

It is well known[12] that the E1 (p-wave) giant resonance of the photonuclear reaction locates in the photon energy region of 15–20 MeV. Here we assume the p-wave photon-absorption cross section as

$$\sigma_p(E_x) = \sigma_r \cdot (E_x/E_r)^{1/2} \cdot \frac{\Gamma^2/4}{\Gamma^2/4 + (E_x - E_r)^2}, \tag{2}$$

where E_r is the resonance energy (15–20 MeV), Γ is the energy width (3–5 MeV) and σ_r is the cross section at E_r. The typical shape of this cross section is illustrated in Fig. 2. We understand that excitation near E_r (~ 15 MeV) is necessary in order to achieve a high reaction rate.

We assume that the excitation by the E1 giant resonance of the multiphoton process will lead to the collective excitation and deformation processes (from spherical to elliptical). For known photonuclear reactions (single photon events) in the E1 giant resonance region of 15–20 MeV gamma-ray energy, (γ, n) reactions open dominantly. In the case of the multiphoton process with low-energy photons (which have energies less than the minimum neutron separation (or binding) energy of 5 MeV for the target nucleus), we may efficiently suppress neutron emission and enhance nuclear deformation to collective excitation levels. In the collective deformation process (elliptical to dumbbell or tandem shape), a fission channel may selectively open. The fission channel is chaotic because of the existence of so many possible combinations of scission fragment pairs. We consider that each scission channel has its own fission potential with different barrier heights

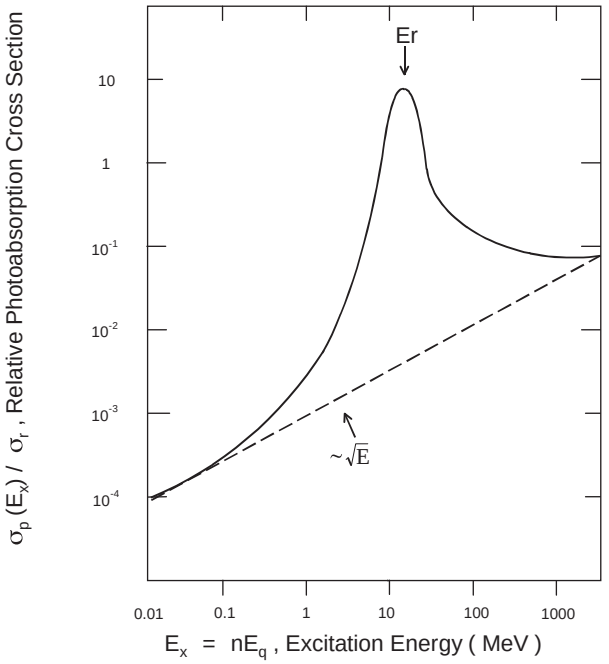

Fig. 2. Assumed cross section of QED photoabsorption of Pd nuclei.

(channel-dependent fission barrier). Defining P_i (E_x) as the channel (i)-dependent tunnel fission probability, the fission cross section can be given as

$$\sigma_f(E_x) = \sigma_p(E_x) \cdot \frac{1}{1} \sum_{i=1}^{I} P_i(E_x). \tag{3}$$

The Wentzel–Kramers–Brillouin (WKB) formula is given later for P_i (E_x).

The reaction rate of the LEPF-SCF process in metal is defined as

$$R(E_q) = N_p \sigma_f(E_x) \cdot \phi_q(E_q) P_q(E_q), \tag{4}$$

where N_p is the number density of Pd isotopes, ϕ_q is the QED photon flux and P_q is the penetration probability of

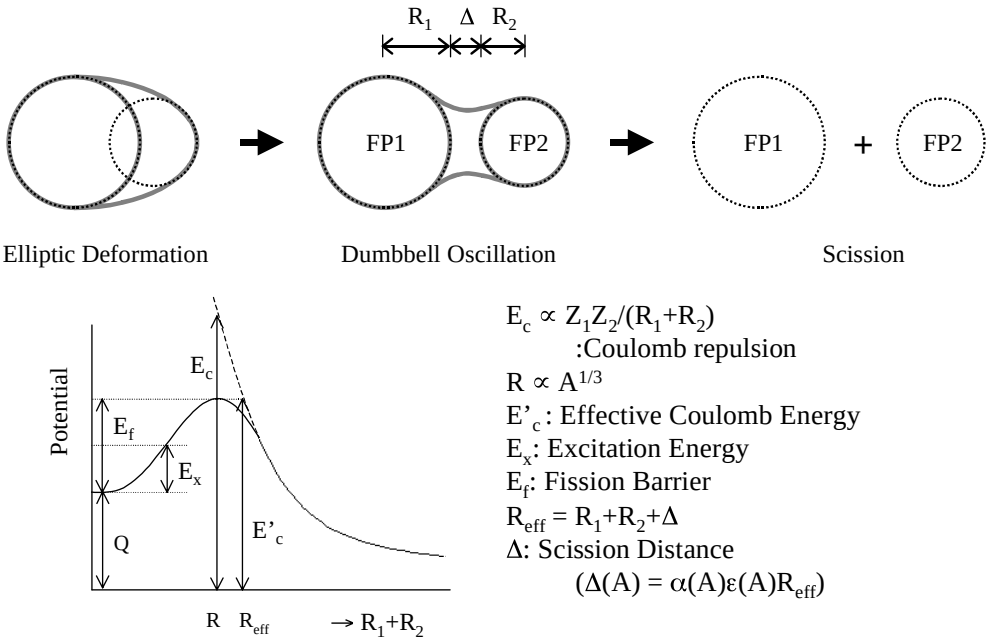

Fig. 3. Tandem (dumbbell dipole) oscillation and scission process.

QED photons. If we assume the situation of PdD_x dynamics of $\phi_q \sim 10^{24}$ photons/(cm^2 s), $N_p = 10^{22}$ atoms/cm^3, $E_x \sim 15$ MeV ($\sim E_f$), and σ_f (E_x) ~ 1 b $= 10^{-24}$ cm^2 and $P_q = 10^{-4}$ (assuming that the average QED photon energy is less than 22 keV of Pd's K-X-ray, a relatively strong attenuation condition to pass the electron cloud of Pd is used here), the fission rate will be:

$$R(E_q) \sim 10^{22} \times 10^{-24} \times 10^{24} \times 10^{-4} = 10^{18}\ \text{fissions/(s cm}^3)(\sim 10\ \text{MW/cm}^3),$$

which is an extremely high rate. Typical values of photofission (single photon event) cross sections around 10 MeV for actinides ($A = 230$–240) are 100–500 mb. If we consider a much milder assumption of $\sim 1\,\mu$b fission cross section where $E_x < E_r$ for medium heavy nuclei, we may obtain ~ 10 W/cm^3 level. Therefore, if LEPF/SCF occurs in $PdD(H)_x$ with positive Q values (5–18 MeV; explained later), we can expect excess power generation as observed in CF experiments.

2.3 Liquid drop model for LEPF

To treat the nuclear fission process, the liquid drop model is conventionally used.[13] The averaged fission barrier is given[13] approximately as

$$E_f \sim \varepsilon^2 A^{2/3}(5.2\text{–}0.117Z^2/A), \tag{5}$$

in MeV unit, where ε is the elliptical deformation coefficient of the nucleus, A is the mass number of the nucleus and Z is the atomic number (number of protons) of the nucleus. The first term on the right-hand side of eq. (5) shows the surface tension which reflects the strength of binding force in the strong interaction, and the second term reflects the Coulomb repulsion. For the U-235 + n to U-236 fission, $\varepsilon \sim 0.3$ and $E_f = 5$ MeV which is below the excited energy level (6.5 MeV) generated by neutron absorption, and therefore prompt fission occurs after n absorption to U-235. To extend the formula to Pd-104, for example, we obtain $E_f = 18.3$ MeV, using $\varepsilon = 0.6$. Because of the much greater surface tension (or strong nuclear binding force) of Pd, we require a much larger deformation force ($\varepsilon = 0.6$) to achieve scission.

The fission process involving LEPF/SCF is illustrated in Fig. 3. The multiphoton E1 absorption excites the elliptical deformation of the nucleus, and for some low E_f channels the tandem (dumbbell) oscillation is collectively induced, leading to the scission of two fragments (FP1 and FP2). The height of fission barrier E_f can be determined by knowing the Q value of the channel and the effective Coulomb energy E_c'. E_c' is estimated by defining the effective scission distance R_{eff}. To obtain R_{eff}, we have to define the ε value (~ 0.6 for Pd) and the jointing factor $\alpha(A)$ which reflects the strength of the jointing force by the strong interaction. For example, we define $\varepsilon = 0.3$ and $\alpha = 0.1$ for U-236 fission and $\varepsilon = 0.6$ and $\alpha = 3.0$ for Pd-LEPF. This estimation was carried out as follows; the point Coulomb repulsive potential is given as

$$V_c(r) = 1.44 Z_1 Z_2 / r, \tag{6}$$

in MeV and fm units. Defining the mutual distance between the FP1 nucleus and the FP2 nucleus as $r = |\boldsymbol{r}_1 - \boldsymbol{r}_2|$ (in fm), the elliptical coefficient can be defined as

$$\varepsilon(r) = (R_1 + R_2 + r - 2R_0)/(2R_0), \tag{7}$$

where R_0, R_1 and R_2 are the radii of the Pd nucleus, FP1 and FP2, respectively, and $R_0 = r_0 A^{1/3}$, $R_1 = r_0 A_1^{1/3}$, $R_2 = r_0 A_2^{1/3}$ with $r_0 = 1.2$ fm. A, A_1 and A_2 are the mass numbers of the Pd nucleus, FP1 and FP2, respectively.

The distortion energy by the deformation is given by[14]

$$\Delta E(r) = [\varepsilon(r)]^2 A^{2/3} \cdot (6.88\text{–}0.14Z^2/A). \tag{8}$$

The change of Coulomb energy by distortion (from the sphere) is

$$\Delta E(r) = -0.14 Z^2 [\varepsilon(r)]^2 A^{-1/3}. \tag{9}$$

At the maximum point of the fission potential curve, fission (scission) occurs, and at that moment the surface ten-

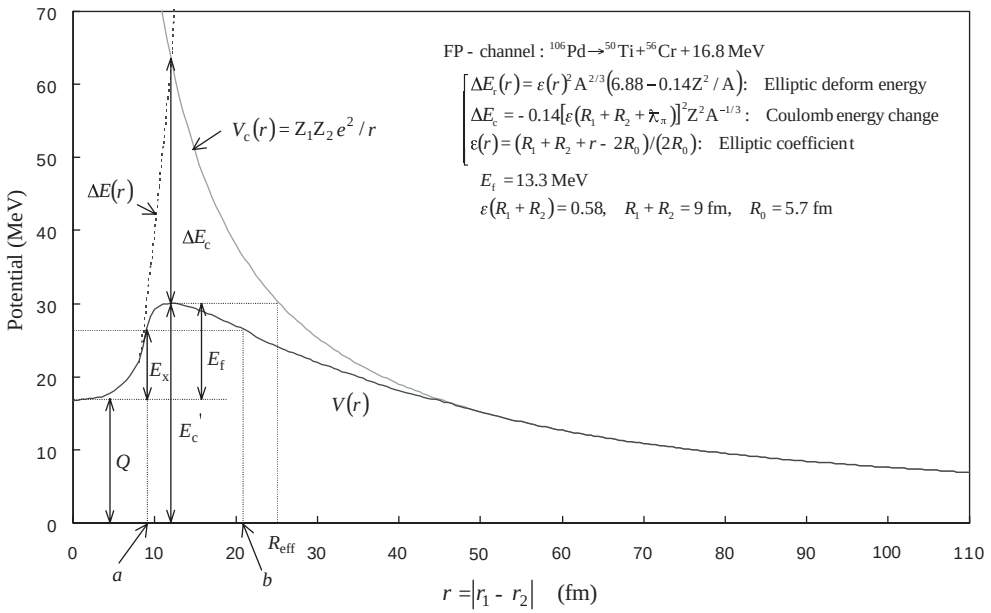

Fig. 4. Fission potential for a scission channel of ^{106}Pd.

sion becomes zero. Therefore, the difference between the point-point Coulomb potential [eq. (6)] and $\Delta E_c(r)$ at $r = R_1 + R_2 + \lambda_\pi$ can give the E_c'-value, where λ_π is the range (about 2 fm) of pions as the force exchange bosons. A fission potential function thus estimated for the $^{106}\text{Pd} \rightarrow {}^{50}\text{Ti} + {}^{56}\text{Cr} + 16.8\,\text{MeV}$ channel is illustrated in Fig. 4. We define the channel-dependent fission barrier E_{fi} by

$$E_{fi} = E'_{ci} - Q_i, \tag{10}$$

and calculate Q_i and E_{ci} for each scission channel. For six Pd isotopes, we have approximately 530 scission channels with positive Q values. Maps of E_{fi} values for Pd isotopes and Au-197 will be shown in the next section.

When the excitation energy E_x is less than E_{fi}, we need to estimate the tunnel fission probability using the following WKB formula:

$$P_i(E_x) = \exp\left[-0.436\sqrt{\mu}\int_a^b (V(r) - E_x)^{1/2}\mathrm{d}r\right], \tag{11}$$

in MeV and fm units, where a and b points are shown in Fig. 4 and $\mu = A_1A_2/(A_1 + A_2)$.

An example of the P_i (E_x) curve is given for the $^{106}\text{Pd} \rightarrow {}^{50}\text{Ti} + {}^{56}\text{Cr} + 16.8\,\text{MeV}$: $E_f = 13.3\,\text{MeV}$ channel, in Fig. 5. For $E_x > E_f$, $P_i(E_x) = 1.0$. We understand that the tunnel fission effect is not negligible but small, and we require excitation close to the E_{fi} values to induce efficient fission.

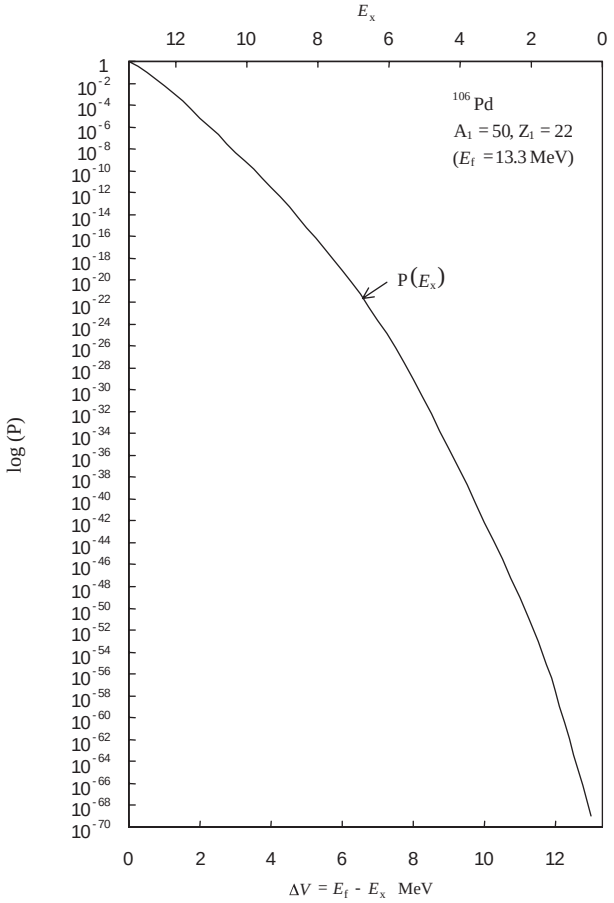

Fig. 5. Tunnel fission probability for a scission channel of $A_1 = 50$ and $Z_1 = 22$ for ^{106}Pd.

3. Fission Products

3.1 General trend

Considering the nuclear chart, namely A (Z, N) plotted vs. N (neutron number: horizontal axis) and Z (atomic number: vertical axis), it is noted that stable isotopes locate along the $N = Z$ the line for low mass region ($A < 60$, for example) and plot a downward bending curve (neutron excess nuclei) for the high mass region. For example: $Z = 20$ and $N = 20$ for ^{40}Ca, $Z = 46$ and $N = 58$ for ^{104}Pd and $Z = 79$ and $N = 118$ for ^{197}Au. ^{235}U is radioactive but very long-lived (half-life of 7×10^8 y) and locates at $Z = 92$ and $N = 143$. Assuming that an FP pair with nearly equal mass is produced by fission, and the FPs of ^{236}U locate around $Z = 46$ and $N = 72$ where short-lived RIs locate in the nuclear chart. Then, the primary fission fragments of ^{236}U are highly radioactive and highly excited (deformed) due to large Q val-

Table I. Scission channels with stable isotope pairs: for example, $Q > 0$.

1-1)	$^{102}\mathrm{Pd} \rightarrow {}^{90}\mathrm{Zr} + {}^{12}\mathrm{C} + 0.84\,\mathrm{MeV}$	($E_\mathrm{f} = 14.3\,\mathrm{MeV}$)
1-2)	$^{102}\mathrm{Pd} \rightarrow {}^{86}\mathrm{Sr} + {}^{16}\mathrm{O} + 1.33\,\mathrm{MeV}$	($E_\mathrm{f} = 17.4\,\mathrm{MeV}$)
1-3)	$^{102}\mathrm{Pd} \rightarrow {}^{78}\mathrm{Se} + {}^{24}\mathrm{Mg} + 3.03\,\mathrm{MeV}$	($E_\mathrm{f} = 21.4\,\mathrm{MeV}$)
1-4)	$^{102}\mathrm{Pd} \rightarrow {}^{74}\mathrm{Ge} + {}^{28}\mathrm{Si} + 6.99\,\mathrm{MeV}$	($E_\mathrm{f} = 19.5\,\mathrm{MeV}$)
1-5)	$^{102}\mathrm{Pd} \rightarrow {}^{70}\mathrm{Zn} + {}^{32}\mathrm{S} + 7.65\,\mathrm{MeV}$	($E_\mathrm{f} = 19.6\,\mathrm{MeV}$)
1-6)	$^{102}\mathrm{Pd} \rightarrow {}^{68}\mathrm{Zn} + {}^{34}\mathrm{S} + 12.01\,\mathrm{MeV}$	($E_\mathrm{f} = 16.1\,\mathrm{MeV}$)
1-7)	$^{102}\mathrm{Pd} \rightarrow {}^{54}\mathrm{Cr} + {}^{48}\mathrm{Ti} + 17.49\,\mathrm{MeV}$	($E_\mathrm{f} = 13.0\,\mathrm{MeV}$)
1-8)	$^{102}\mathrm{Pd} \rightarrow {}^{54}\mathrm{Fe} + {}^{48}\mathrm{Ca} + 12.54\,\mathrm{MeV}$	($E_\mathrm{f} = 17.5\,\mathrm{MeV}$)
1-9)	$^{102}\mathrm{Pd} \rightarrow {}^{53}\mathrm{Cr} + {}^{49}\mathrm{Ti} + 15.91\,\mathrm{MeV}$	($E_\mathrm{f} = 14.6\,\mathrm{MeV}$)
1-10)	$^{104}\mathrm{Pd} \rightarrow {}^{88}\mathrm{Sr} + {}^{16}\mathrm{O} + 3.26\,\mathrm{MeV}$	($E_\mathrm{f} = 15.4\,\mathrm{MeV}$)
1-11)	$^{104}\mathrm{Pd} \rightarrow {}^{84}\mathrm{Kr} + {}^{20}\mathrm{Ne} + 0.08\,\mathrm{MeV}$	($E_\mathrm{f} = 21.7\,\mathrm{MeV}$)
1-12)	$^{104}\mathrm{Pd} \rightarrow {}^{80}\mathrm{Se} + {}^{24}\mathrm{Mg} + 2.31\,\mathrm{MeV}$	($E_\mathrm{f} = 22.0\,\mathrm{MeV}$)
1-13)	$^{104}\mathrm{Pd} \rightarrow {}^{76}\mathrm{Ge} + {}^{28}\mathrm{Si} + 5.31\,\mathrm{MeV}$	($E_\mathrm{f} = 21.1\,\mathrm{MeV}$)
1-14)	$^{104}\mathrm{Pd} \rightarrow {}^{56}\mathrm{Fe} + {}^{48}\mathrm{Ca} + 15.42\,\mathrm{MeV}$	($E_\mathrm{f} = 14.5\,\mathrm{MeV}$)
1-15)	$^{104}\mathrm{Pd} \rightarrow {}^{54}\mathrm{Cr} + {}^{50}\mathrm{Ti} + 18.76\,\mathrm{MeV}$	($E_\mathrm{f} = 11.4\,\mathrm{MeV}$)
1-16)	$^{104}\mathrm{Pd} \rightarrow {}^{64}\mathrm{Ni} + {}^{40}\mathrm{Ar} + 12.74\,\mathrm{MeV}$	($E_\mathrm{f} = 16.4\,\mathrm{MeV}$)
1-17)	$^{105}\mathrm{Pd} \rightarrow {}^{57}\mathrm{Fe} + {}^{48}\mathrm{Ca} + 17.32\,\mathrm{MeV}$	($E_\mathrm{f} = 13.8\,\mathrm{MeV}$)
1-18)	$^{106}\mathrm{Pd} \rightarrow {}^{58}\mathrm{Fe} + {}^{48}\mathrm{Ca} + 16.46\,\mathrm{MeV}$	($E_\mathrm{f} = 13.2\,\mathrm{MeV}$)
1-19)	$^{106}\mathrm{Pd} \rightarrow {}^{82}\mathrm{Se} + {}^{24}\mathrm{Mg} + 1.68\,\mathrm{MeV}$	($E_\mathrm{f} = 22.6\,\mathrm{MeV}$)
1-20)	$^{106}\mathrm{Pd} \rightarrow {}^{86}\mathrm{Kr} + {}^{20}\mathrm{Ne} + 0.40\,\mathrm{MeV}$	($E_\mathrm{f} = 21.2\,\mathrm{MeV}$)

Table II. Scission channels with finally stable FPs via pure β^--decay: for example, $Q > 0$.

2-1)	$^{102}\mathrm{Pd} \rightarrow {}^{57}\mathrm{Fe} + {}^{45}\mathrm{Ca}(162.6\,\mathrm{d}:\beta^-){}^{45}\mathrm{Sc} + 13.06\,\mathrm{MeV}$	($E_\mathrm{f} = 17.0\,\mathrm{MeV}$)
2-2)	$^{102}\mathrm{Pd} \rightarrow {}^{66}\mathrm{Ni}(2.38\,\mathrm{d}:\beta^-){}^{66}\mathrm{Zn} + {}^{36}\mathrm{Ar} + 8.33\,\mathrm{MeV}$	($E_\mathrm{f} = 21.1\,\mathrm{MeV}$)
2-3)	$^{102}\mathrm{Pd} \rightarrow {}^{62}\mathrm{Fe}(1.13\,\mathrm{m}:\beta^-){}^{62}\mathrm{Ni} + {}^{40}\mathrm{Ca} + 5.82\,\mathrm{MeV}$	($E_\mathrm{f} = 24.4\,\mathrm{MeV}$)
2-4)	$^{102}\mathrm{Pd} \rightarrow {}^{55}\mathrm{Mn} + {}^{47}\mathrm{Sc}(3.35\,\mathrm{d}:\beta^-){}^{47}\mathrm{Ti} + 14.11\,\mathrm{MeV}$	($E_\mathrm{f} = 16.2\,\mathrm{MeV}$)
2-5)	$^{104}\mathrm{Pd} \rightarrow {}^{68}\mathrm{Ni}(9.25\,\mathrm{m}:\beta^-){}^{68}\mathrm{Zn} + {}^{36}\mathrm{Ar} + 4.32\,\mathrm{MeV}$	($E_\mathrm{f} = 24.9\,\mathrm{MeV}$)
2-6)	$^{104}\mathrm{Pd} \rightarrow {}^{65}\mathrm{Co}(1.25\,\mathrm{s}:\beta^-){}^{65}\mathrm{Cu} + {}^{39}\mathrm{K} + 3.58\,\mathrm{MeV}$	($E_\mathrm{f} = 26.1\,\mathrm{MeV}$)
2-7)	$^{106}\mathrm{Pd} \rightarrow {}^{62}\mathrm{Fe}(1.13\,\mathrm{m}:\beta^-){}^{62}\mathrm{Ni} + {}^{44}\mathrm{Ca} + 10.46\,\mathrm{MeV}$	($E_\mathrm{f} = 19.3\,\mathrm{MeV}$)
2-8)	$^{106}\mathrm{Pd} \rightarrow {}^{54}\mathrm{Ti}(1.5\,\mathrm{s}:\beta^-){}^{54}\mathrm{V}(49.8\,\mathrm{s}:\beta^-){}^{54}\mathrm{Cr} + {}^{52}\mathrm{Cr} + 11.11\,\mathrm{MeV}$	($E_\mathrm{f} = 19.0\,\mathrm{MeV}$)
2-9)	$^{105}\mathrm{Pd} \rightarrow {}^{55}\mathrm{Cr}(3.5\,\mathrm{m}:\beta^-){}^{55}\mathrm{Mn} + {}^{50}\mathrm{Ti} + 18.12\,\mathrm{MeV}$	($E_\mathrm{f} = 12.1\,\mathrm{MeV}$)
2-10)	$^{105}\mathrm{Pd} \rightarrow {}^{69}\mathrm{Zn}(13.8\,\mathrm{h}:\beta^-){}^{69}\mathrm{Ga} + {}^{36}\mathrm{S} + 10.66\,\mathrm{MeV}$	($E_\mathrm{f} = 17.1\,\mathrm{MeV}$)

ues (180–190 MeV) of scissions and relatively weak surface tension (weak jointing factor), and promptly emit one or two neutrons and γ-rays to transit to ground-states which make succeeding β-decays (mostly short-lived) to reach stable or long-lived isotopes. One might be prejudiced that fission produces mostly radioactive dirty products, but in fact the data on fission fragments for $^{235}\mathrm{U} + n$ fission[15] shows that stable isotopes of final FPs are dominant at two peaks (around $A = 92$ and $A = 144$) of mass distribution and RIs form a minor group. Thermal neutron fission in ^{235}U is analyzed elsewhere.[16] Assuming fission of a Pd isotope, where a nearly equal mass FP pair locates around $Z = 23$ and $A = 52$, then their location is very close to the belt of stable isotopes. Therefore, we presume that LEPF of Pd isotopes may produce dominant stable isotopes. Since the surface tension (or jointing force) for a Pd liquid drop is much stronger than that of U and the Q values are rather small (< 18 MeV), fission fragments may promptly become spherical (ground-state: notdeformed) to form stable isotopes or short-lived β^--decays, and reach stable isotopes in a short time.

Stable FP isotopes are generated during Pd-LEPF in the following three ways; 1) scission channels of stable FP isotope pairs (example is shown in Table I), 2) scission channels of short-lived RIs with pure β^--decay (examples are shown in Table II) and 3) scission channels of short-lived RIs with partial γ-emissions in β^--decays (examples are shown in Table III). Examples are given for exothermic reactions ($Q > 0$), and calculated fission barriers (E_f values) are also given. Scission channels with underlined E_f values are within the lowest band (LB1) as explained later. In the case of Pd, we list 530 channels for $Q > 0$.

For reaction channels with negative (endothermic) Q values, LEPF does not occur due to very large fission barriers (30–55 MeV), compared with the E1 resonance energy ($E_\mathrm{r} \sim 15$ MeV). The scission channels emitting neutrons, ^{4}He and ^{8}Be, are all endothermic ($Q < 0$). Therefore, we conclude that there are no emissions of neutrons and α-particles in Pd-LEPF/SCF.

3.2 Channel-dependent fission barriers

Channel-dependent fission barriers calculated using eq. (10) are plotted as a function of mass number of FP. Two symmetric points against A/2 are plotted for each scission channel. Results are shown in Figs. 6(a)–6(f), respectively, for Pd-102, Pd-104, Pd-105, Pd-106, Pd-108 and Pd-110. In the figures, two band lines (LB1 and LB2) are plotted to show the assumed lowest band of channel-dependent fission barriers. Considering the E1 photonuclear resonance energy

Table III. Scission channels with finally stable FPs via short-lived β^--decay with partial γ-ray emission; for example, $Q > 0$.

3-1)	$^{104}\mathrm{Pd} \rightarrow {}^{51}\mathrm{V} + {}^{53}\mathrm{V}(1.6\,\mathrm{m} : \beta^-, E_\gamma = 1.01\,\mathrm{MeV}){}^{53}\mathrm{Cr} + 14.65\,\mathrm{MeV}$	($E_\mathrm{f} = 15.7\,\mathrm{MeV}$)
3-2)	$^{104}\mathrm{Pd} \rightarrow {}^{53}\mathrm{Cr} + {}^{51}\mathrm{Ti}(5.76\,\mathrm{m} : \beta^-, E_\gamma = 0.32\,\mathrm{MeV}){}^{51}\mathrm{V} + 15.62\,\mathrm{MeV}$	($E_\mathrm{f} = 14.7\,\mathrm{MeV}$)
3-3)	$^{104}\mathrm{Pd} \rightarrow {}^{72}\mathrm{Zn}(1.94\,\mathrm{d} : \beta^-, E_\gamma = 0.16\,\mathrm{MeV}){}^{72}\mathrm{Ga}(14\,\mathrm{h}){}^{72}\mathrm{Ga} + {}^{32}\mathrm{S} + 4.75\,\mathrm{MeV}$	($E_\mathrm{f} = 23.3\,\mathrm{MeV}$)
3-4)	$^{108}\mathrm{Pd} \rightarrow {}^{50}\mathrm{Ti} + {}^{58}\mathrm{Cr}(7\,\mathrm{s} : \beta^-, E_\gamma = 0.81\,\mathrm{MeV}){}^{58}\mathrm{Fe} + 17.80\,\mathrm{MeV}$	($E_\mathrm{f} = 16.2\,\mathrm{MeV}$)
3-5)	$^{108}\mathrm{Pd} \rightarrow {}^{64}\mathrm{Ni} + {}^{44}\mathrm{Ar}(12\,\mathrm{m} : \beta^-, E_\gamma = 1.89\,\mathrm{MeV}){}^{44}\mathrm{K} + 9.84\,\mathrm{MeV}$	($E_\mathrm{f} = 18.9\,\mathrm{MeV}$)
3-6)	$^{110}\mathrm{Pd} \rightarrow {}^{54}\mathrm{Cr} + {}^{56}\mathrm{Ti}(1.2\,\mathrm{s} : \beta^-){}^{56}\mathrm{Mn}^*(2.5\,\mathrm{h}){}^{56}\mathrm{Fe} + 7.68\,\mathrm{MeV}$	($E_\mathrm{f} = 22.1\,\mathrm{MeV}$)
3-7)	$^{105}\mathrm{Pd} \rightarrow {}^{64}\mathrm{Ni} + {}^{40}\mathrm{Ar}(1.8\,\mathrm{h} : \beta^-, E_\gamma = 1.29\,\mathrm{MeV}){}^{41}\mathrm{K} + 11.75\,\mathrm{MeV}$	($E_\mathrm{f} = 17.3\,\mathrm{MeV}$)
3-8)	$^{105}\mathrm{Pd} \rightarrow {}^{59}\mathrm{Co} + {}^{46}\mathrm{K}(1.75\,\mathrm{m} : \beta^-, E_\gamma = 1.346\,\mathrm{MeV}){}^{46}\mathrm{Ca} + 9.23\,\mathrm{MeV}$	($E_\mathrm{f} = 14.4\,\mathrm{MeV}$)
3-9)	$^{105}\mathrm{Pd} \rightarrow {}^{56}\mathrm{Fe} + {}^{49}\mathrm{Ca}(8.7\,\mathrm{m} : \beta^-, E_\gamma = 3.084\,\mathrm{MeV}){}^{49}\mathrm{Ti}{}^{49}\mathrm{Sc}^*(57\,\mathrm{m}){}^{49}\mathrm{Ti} + 13.48\,\mathrm{MeV}$	($E_\mathrm{f} = 16.3\,\mathrm{MeV}$)
3-10)	$^{105}\mathrm{Pd} \rightarrow {}^{54}\mathrm{Cr} + {}^{51}\mathrm{Ti}(5.76\,\mathrm{m} : \beta^-, E_\gamma = 0.320\,\mathrm{MeV}){}^{51}\mathrm{V} + 18.24\,\mathrm{MeV}$	($E_\mathrm{f} = 11.2\,\mathrm{MeV}$)
3-11)	$^{105}\mathrm{Pd} \rightarrow {}^{53}\mathrm{Cr} + {}^{52}\mathrm{Ti}(1.7\,\mathrm{m} : \beta^-, E_\gamma = 0.124\,\mathrm{MeV}){}^{52}\mathrm{V}(3.7\,\mathrm{m}){}^{52}\mathrm{Cr} + 16.33\,\mathrm{MeV}$	($E_\mathrm{f} = 13.9\,\mathrm{MeV}$)
3-12)	$^{105}\mathrm{Pd} \rightarrow {}^{51}\mathrm{V} + {}^{54}\mathrm{V}(50\,\mathrm{s} : \beta^-, E_\gamma = 4.083\,\mathrm{MeV}){}^{54}\mathrm{Cr} + 13.67\,\mathrm{MeV}$	($E_\mathrm{f} = 16.6\,\mathrm{MeV}$)
3-13)	$^{105}\mathrm{Pd} \rightarrow {}^{41}\mathrm{K} + {}^{64}\mathrm{Co}(0.3\,\mathrm{s} : \beta^-, E_\gamma = 1.345\,\mathrm{MeV}){}^{64}\mathrm{Ni} + 6.93\,\mathrm{MeV}$	($E_\mathrm{f} = 22.6\,\mathrm{MeV}$)
3-14)	$^{105}\mathrm{Pd} \rightarrow {}^{40}\mathrm{Ar} + {}^{65}\mathrm{Ni}(2.5\,\mathrm{h} : \beta^-, E_\gamma = 0.77\,\mathrm{MeV}){}^{65}\mathrm{Cu} + 11.75\,\mathrm{MeV}$	($E_\mathrm{f} = 17.3\,\mathrm{MeV}$)
3-15)	$^{105}\mathrm{Pd} \rightarrow {}^{37}\mathrm{Cl} + {}^{68}\mathrm{Cu}(31\,\mathrm{s} : \beta^-, E_\gamma = 1.077\,\mathrm{MeV}){}^{65}\mathrm{Zn} + 8.59\,\mathrm{MeV}$	($E_\mathrm{f} = 19.6\,\mathrm{MeV}$)
3-16)	$^{106}\mathrm{Pd} \rightarrow {}^{50}\mathrm{Ti} + {}^{56}\mathrm{Cr}(6\,\mathrm{m} : \beta^-){}^{56}\mathrm{Mn}(2.6\,\mathrm{h} : \beta^-, E_\gamma = 0.847\,\mathrm{MeV}, E_\gamma = 1.811\,\mathrm{MeV}){}^{56}\mathrm{Fe} + 16.81\,\mathrm{MeV}$	($E_\mathrm{f} = 13.32\,\mathrm{MeV}$)
3-17)	$^{106}\mathrm{Pd} \rightarrow {}^{52}\mathrm{Ti}(1.7\,\mathrm{m} : \beta^-, E_\gamma = 0.124\,\mathrm{MeV}){}^{52}\mathrm{V}(3.7\,\mathrm{m} : \beta^-, E_\gamma = 1.434\,\mathrm{MeV}){}^{52}\mathrm{Cr} + {}^{54}\mathrm{Cr} + 16.49\,\mathrm{MeV}$	($E_\mathrm{f} = 13.63\,\mathrm{MeV}$)
3-18)	$^{104}\mathrm{Pd} \rightarrow {}^{52}\mathrm{Ti}(1.7\,\mathrm{m} : \beta^-, E_\gamma = 0.124\,\mathrm{MeV}){}^{52}\mathrm{Cr} + {}^{52}\mathrm{Cr} + 15.49\,\mathrm{MeV}$	($E_\mathrm{f} = 14.83\,\mathrm{MeV}$)
3-19)	$^{104}\mathrm{Pd} \rightarrow {}^{51}\mathrm{Ti}(5.8\,\mathrm{m} : \beta^-, E_\gamma = 0.320\,\mathrm{MeV}){}^{51}\mathrm{V} + {}^{53}\mathrm{Cr} + 15.62\,\mathrm{MeV}$	($E_\mathrm{f} = 14.70\,\mathrm{MeV}$)

Table IV. List of top ten channels opening first for LEPF of Pd.

(1)	$^{104}\mathrm{Pd} \rightarrow {}^{50}\mathrm{Ti} + {}^{54}\mathrm{Cr} + 18.96\,\mathrm{MeV}$	($E_\mathrm{f} = 11.36\,\mathrm{MeV}$)
(2)	$^{102}\mathrm{Pd} \rightarrow {}^{50}\mathrm{Ti} + {}^{52}\mathrm{Cr} + 18.91\,\mathrm{MeV}$	($E_\mathrm{f} = 11.60\,\mathrm{MeV}$)
(3)	$^{105}\mathrm{Pd} \rightarrow {}^{51}\mathrm{Ti}(5.8\,\mathrm{m}){}^{51}\mathrm{V} + {}^{54}\mathrm{Cr} + 18.24\,\mathrm{MeV}$	($E_\mathrm{f} = 11.98\,\mathrm{MeV}$)
(4)	$^{105}\mathrm{Pd} \rightarrow {}^{50}\mathrm{Ti} + {}^{55}\mathrm{Cr}(3.5\,\mathrm{m}){}^{55}\mathrm{Mn} + 18.12\,\mathrm{MeV}$	($E_\mathrm{f} = 12.11\,\mathrm{MeV}$)
(5)	$^{102}\mathrm{Pd} \rightarrow {}^{48}\mathrm{Ti} + {}^{54}\mathrm{Cr} + 17.49\,\mathrm{MeV}$	($E_\mathrm{f} = 13.03\,\mathrm{MeV}$)
(6)	$^{106}\mathrm{Pd} \rightarrow {}^{48}\mathrm{Ca} + {}^{58}\mathrm{Fe} + 16.46\,\mathrm{MeV}$	($E_\mathrm{f} = 13.23\,\mathrm{MeV}$)
(7)	$^{106}\mathrm{Pd} \rightarrow {}^{50}\mathrm{Ti} + {}^{56}\mathrm{Cr}(6\,\mathrm{m}){}^{56}\mathrm{Mn}(2.6\,\mathrm{h}){}^{56}\mathrm{Fe} + 16.81\,\mathrm{MeV}$	($E_\mathrm{f} = 13.32\,\mathrm{MeV}$)
(8)	$^{108}\mathrm{Pd} \rightarrow {}^{48}\mathrm{Ca} + {}^{60}\mathrm{Fe}(1.6 \times 10^6\,\mathrm{y})^* + 16.10\,\mathrm{MeV}$	($E_\mathrm{f} = 13.42\,\mathrm{MeV}$)
(9)	$^{106}\mathrm{Pd} \rightarrow {}^{52}\mathrm{Ti}(1.7\,\mathrm{m}){}^{52}\mathrm{V}(3.7\,\mathrm{m}){}^{52}\mathrm{Cr} + {}^{54}\mathrm{Cr} + 16.49\,\mathrm{MeV}$	($E_\mathrm{f} = 13.63\,\mathrm{MeV}$)
(10)	$^{105}\mathrm{Pd} \rightarrow {}^{48}\mathrm{Ca} + {}^{57}\mathrm{Fe} + 15.98\,\mathrm{MeV}$	($E_\mathrm{f} = 13.81\,\mathrm{MeV}$)

$E_\mathrm{r} \sim 15\,\mathrm{MeV}$ and its width $\Gamma \sim 4\,\mathrm{MeV}$, the lower level lines are given at 18 MeV for LB1 and at 20 MeV for LB2. The upper level line is set at $E_\mathrm{r} - \Gamma = 11\,\mathrm{MeV}$ which is slightly above the lowest E_f-value (for ^{104}Pd).

It is interesting to find characteristic patterns of E_f distributions for different Pd isotopes. In particular, around mass = 50, we observed a void-gap near 20 MeV which is clearly apparent for Pd-102, Pd-105 and Pd-106, which may reflect the shell effect of the nuclear structure of each Pd isotope.

Considering the degree of photonuclear excitation (E_x value) which may correspond to experimental conditions, we find that the scission channels with the lowest E_f values open first for ^{102}Pd and ^{104}Pd and other channels with larger E_f values subsequently open for ^{102}Pd, ^{104}Pd, ^{105}Pd and ^{106}Pd. The contributions of ^{108}Pd and ^{110}Pd are small due to their higher E_f values and their smaller number of channels within LB; for example, the numbers of scission channels within the LB1 belt are 20, 21, 23, 13, 12 and 5, respectively, for ^{102}Pd, ^{104}Pd, ^{105}Pd, ^{106}Pd, ^{108}Pd and ^{110}Pd. We also note that channels within LB1 and LB2 locate densely around $A = 50$, which suggests the shape of the mass distribution of fission products.

The list of the top ten fission channels opening first for Pd-LEPF is given in Table IV. For this ranking, we ignored the differences in the degree of multiphoton absorption for different Pd isotopes and made slice-cuts using only E_f values, although some isotopes (such as ^{102}Pd and ^{104}Pd) might be most efficiently excited to near $E_\mathrm{r} = 15\,\mathrm{MeV}$ levels. The tier-2 ranking for the 11th to 30th E_f values is given in Table V. We can extract several important results from Tables IV and V.

1) Eleven channels out of the top 20 produce directly stable FP isotopes and eight out of these 20 produce finally stable isotopes.
2) The dominant even-Z elements of stable FPs are Ti, Cr, Fe and Ca, and naturally non abundant isotopes such as ^{44}Ca, ^{46}Ca, ^{48}Ca, ^{49}Ti, ^{50}Ti, ^{53}Cr, ^{54}Cr, ^{57}Fe and ^{58}Fe are dominantly produced.
3) Relatively minor production of odd-Z elements is observed for ^{51}V, ^{55}Mn and ^{59}Co.
4) Production of the long-lived (1.5×10^6 y) iron isotope ^{60}Fe may be a good indicator for checking Pd-LEPF, since ^{60}Fe decays with β^- (100% transition to 58.59 keV; 2+ state) and 58.59 keV [γ-ray emission (10 min half-life)].

Since these results are unusual and characteristic to Pd-LEPF/SCF, thorough testing by experiments is required. Analyses of dominant elements (Z-distribution) and isotopic ratios are of interest.

Iwamura *et al.*[4] have reported the dominant production

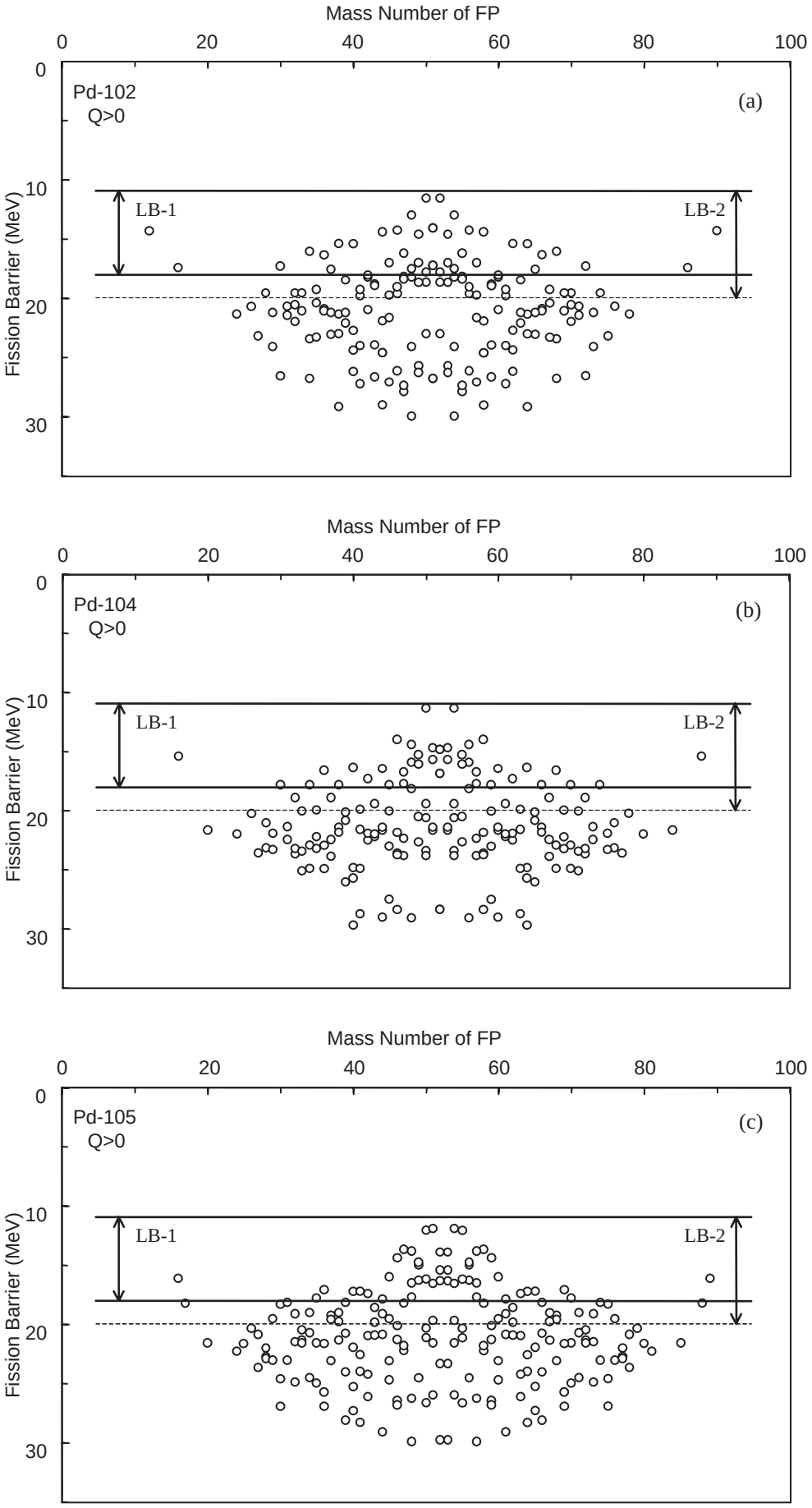

Fig. 6. Pattern of channel-dependent fission barriers for ^{102}Pd (a), ^{104}Pd (b), ^{105}Pd (c), ^{106}Pd (d), ^{108}Pd (e), ^{110}Pd (f).

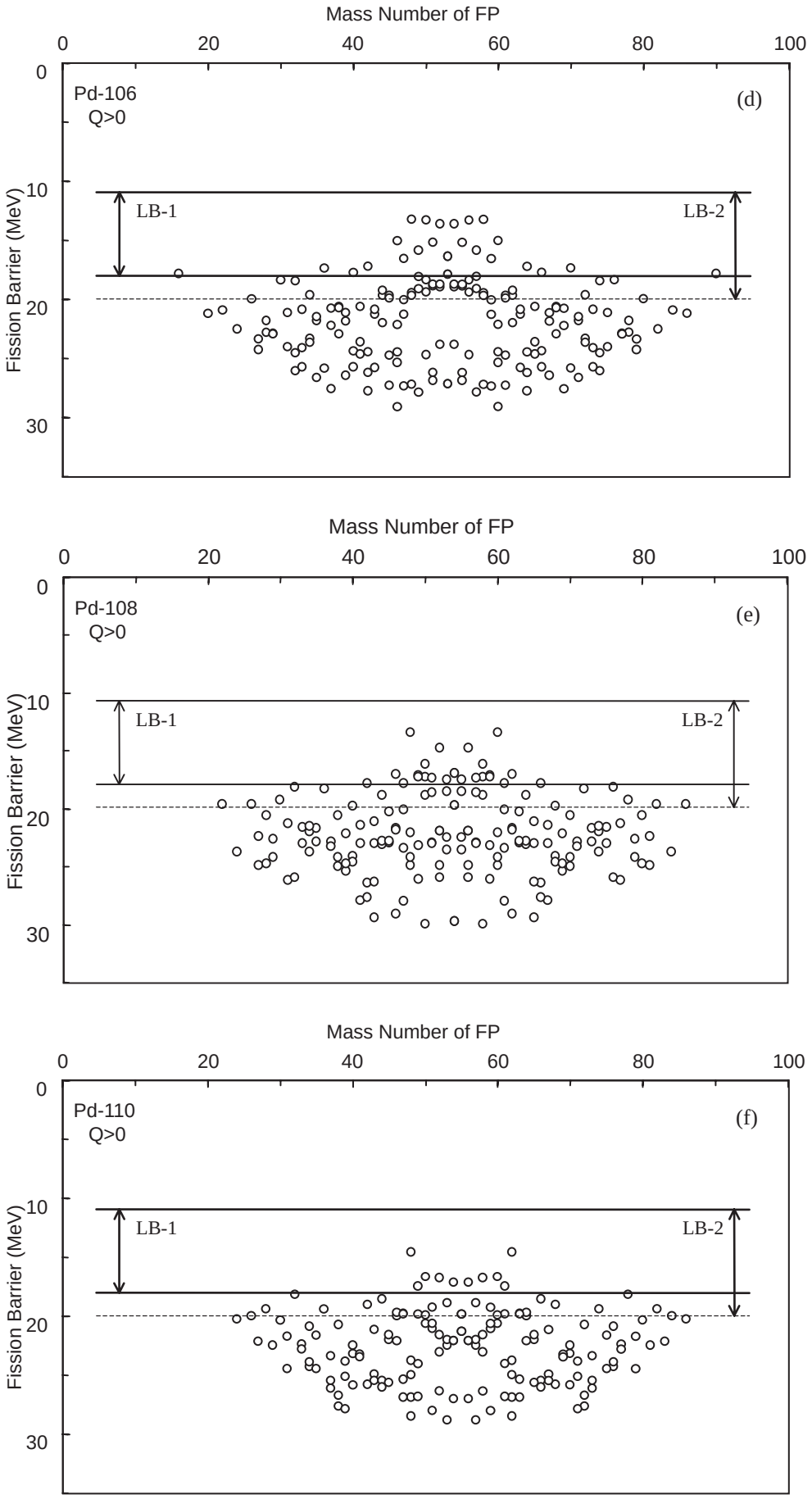

Fig. 6. *Continued.*

Table V. List of rank-2 channels for LEPF of Pd.

(11)	$^{105}\mathrm{Pd} \rightarrow {}^{47}\mathrm{Ca}(4.5\,\mathrm{d})^{47}\mathrm{Sc}(3.3\,\mathrm{d})^{47}\mathrm{Ti} + {}^{58}\mathrm{Fe} + 16.07\,\mathrm{MeV}$	($E_\mathrm{f} = 13.72\,\mathrm{MeV}$)
(12)	$^{105}\mathrm{Pd} \rightarrow {}^{52}\mathrm{Ti}(1.7\,\mathrm{m})^{52}\mathrm{V}(3.7\,\mathrm{m})^{52}\mathrm{Cr} + {}^{53}\mathrm{Cr} + 16.33\,\mathrm{MeV}$	($E_\mathrm{f} = 13.89\,\mathrm{MeV}$)
(13)	$^{104}\mathrm{Pd} \rightarrow {}^{46}\mathrm{Ca} + {}^{58}\mathrm{Fe} + 15.89\,\mathrm{MeV}$	($E_\mathrm{f} = 14.01\,\mathrm{MeV}$)
(14)	$^{102}\mathrm{Pd} \rightarrow {}^{51}\mathrm{V} + {}^{51}\mathrm{V} + 16.47\,\mathrm{MeV}$	($E_\mathrm{f} = 14.10\,\mathrm{MeV}$)
(15)	$^{102}\mathrm{Pd} \rightarrow {}^{46}\mathrm{Ca} + {}^{56}\mathrm{Fe} + 15.81\,\mathrm{MeV}$	($E_\mathrm{f} = 14.27\,\mathrm{MeV}$)
(16)	$^{102}\mathrm{Pd} \rightarrow {}^{44}\mathrm{Ca} + {}^{58}\mathrm{Fe} + 15.69\,\mathrm{MeV}$	($E_\mathrm{f} = 14.42\,\mathrm{MeV}$)
(17)	$^{105}\mathrm{Pd} \rightarrow {}^{46}\mathrm{Ca} + {}^{59}\mathrm{Fe}(44\,\mathrm{d})^{59}\mathrm{Co} + 15.38\,\mathrm{MeV}$	($E_\mathrm{f} = 14.43\,\mathrm{MeV}$)
(18)	$^{104}\mathrm{Pd} \rightarrow {}^{48}\mathrm{Ca} + {}^{56}\mathrm{Fe} + 15.42\,\mathrm{MeV}$	($E_\mathrm{f} = 14.45\,\mathrm{MeV}$)
(19)	$^{110}\mathrm{Pd} \rightarrow {}^{48}\mathrm{Ca} + {}^{62}\mathrm{Fe}(1.1\,\mathrm{m})^{62}\mathrm{Co}(14\,\mathrm{m})^{62}\mathrm{Ni} + 14.76\,\mathrm{MeV}$	($E_\mathrm{f} = 14.59\,\mathrm{MeV}$)
(20)	$^{102}\mathrm{Pd} \rightarrow {}^{49}\mathrm{Ti} + {}^{53}\mathrm{Cr} + 15.91\,\mathrm{MeV}$	($E_\mathrm{f} = 14.60\,\mathrm{MeV}$)
(21)	$^{104}\mathrm{Pd} \rightarrow {}^{51}\mathrm{Ti}(5.8\,\mathrm{m})^{51}\mathrm{V} + {}^{53}\mathrm{Cr} + 15.62\,\mathrm{MeV}$	($E_\mathrm{f} = 14.70\,\mathrm{MeV}$)
(22)	$^{108}\mathrm{Pd} \rightarrow {}^{52}\mathrm{Ti}(1.7\,\mathrm{m})^{52}\mathrm{V}(3.7\,\mathrm{m})^{52}\mathrm{Cr} + {}^{56}\mathrm{Cr}(6\,\mathrm{m})^{56}\mathrm{Mn}(2.6\,\mathrm{h})^{56}\mathrm{Fe} + 15.23\,\mathrm{MeV}$	($E_\mathrm{f} = 14.71\,\mathrm{MeV}$)
(23)	$^{105}\mathrm{Pd} \rightarrow {}^{49}\mathrm{Ti} + {}^{56}\mathrm{Cr}(6\,\mathrm{m})^{56}\mathrm{Mn}(2.6\,\mathrm{h})^{56}\mathrm{Fe} + 15.43\,\mathrm{MeV}$	($E_\mathrm{f} = 14.80\,\mathrm{MeV}$)
(24)	$^{104}\mathrm{Pd} \rightarrow {}^{52}\mathrm{Ti}(1.7\,\mathrm{m})^{52}\mathrm{Cr} + {}^{52}\mathrm{Cr} + 15.49\,\mathrm{MeV}$	($E_\mathrm{f} = 14.83\,\mathrm{MeV}$)
(25)	$^{105}\mathrm{Pd} \rightarrow {}^{49}\mathrm{Sc}(57\,\mathrm{m})^{49}\mathrm{Ti} + {}^{56}\mathrm{Mn}(2.6\,\mathrm{h})^{56}\mathrm{Fe} + 15.04\,\mathrm{MeV}$	($E_\mathrm{f} = 15.02\,\mathrm{MeV}$)
(26)	$^{106}\mathrm{Pd} \rightarrow {}^{46}\mathrm{Ca} + {}^{60}\mathrm{Fe}(1.5 \times 10^6 y)^* + 14.64\,\mathrm{MeV}$	($E_\mathrm{f} = 15.09\,\mathrm{MeV}$)
(27)	$^{106}\mathrm{Pd} \rightarrow {}^{51}\mathrm{Ti}(5.8\,\mathrm{m})^{51}\mathrm{V} + {}^{55}\mathrm{Cr}(3.5\,\mathrm{m})^{55}\mathrm{Mn} + 14.93\,\mathrm{MeV}$	($E_\mathrm{f} = 15.20\,\mathrm{MeV}$)
(28)	$^{104}\mathrm{Pd} \rightarrow {}^{49}\mathrm{Sc}(57\,\mathrm{m})^{49}\mathrm{Ti} + {}^{55}\mathrm{Mn} + 14.87\,\mathrm{MeV}$	($E_\mathrm{f} = 15.29\,\mathrm{MeV}$)
(29)	$^{105}\mathrm{Pd} \rightarrow {}^{52}\mathrm{V}(3.7\,\mathrm{m})^{52}\mathrm{Cr} + {}^{53}\mathrm{V}(1.6\,\mathrm{m})^{53}\mathrm{Cr} + 14.87\,\mathrm{MeV}$	($E_\mathrm{f} = 15.41\,\mathrm{MeV}$)
(30)	$^{102}\mathrm{Pd} \rightarrow {}^{40}\mathrm{Ar} + {}^{62}\mathrm{Ni} + 13.86\,\mathrm{MeV}$	($E_\mathrm{f} = 15.42\,\mathrm{MeV}$)

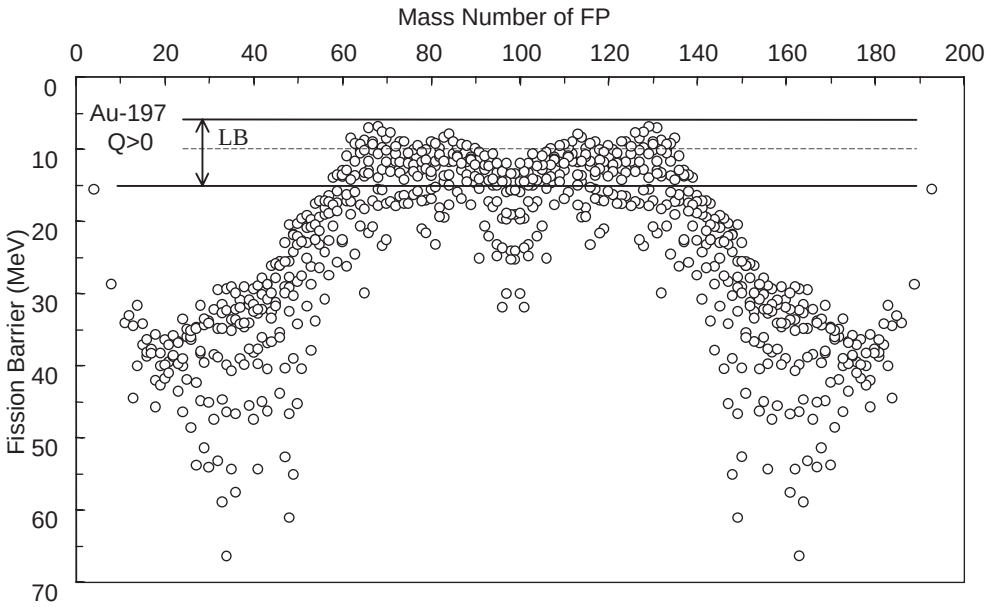

Fig. 7. Pattern of channel-dependent fission barriers for ^{197}Au.

of Ca, Ti, Cr and Fe in their D_2O/multilayered Pd experiments with EDX and WDX analyses. They also reported anomalously enhanced (more than 10 times the value of natural abundance) isotopic ratios for ^{57}Fe/^{56}Fe/ and ^{58}Fe/^{56}Fe. These experimental results agree very well with the present theoretical results [items 1) and 2)].

In the rank-4 channel, ^{55}Cr (3.5 m) decays with pure β^- ($Q_\beta = 2603\,\mathrm{keV}$) emission but it is difficult to detect its radiation from outside the CF electrolysis cell due to the attenuation of β-rays. However, for the rank-3 channel, ^{51}Ti (5.8 m) decays with 92% branching of β-emission ($Q_\beta = 2470.7\,\mathrm{keV}$) to 320 keV, which has the $5/2^-$ level which emits 320 keV γ-rays in 184 ps and should be detected *in situ*, if ^{105}Pd is to be efficiently photoexcited to the E_r level. We present similar discussions for the rank-7, -9, -11, -12, -17, -19, -21 and -22 channels. Therefore, the possibility of short-lived γ-ray emission in Pd-LEPF depends largely on the degree of photoexcitation for ^{105}Pd (and other elements similar to Pd-104 and Pd-106). If ^{105}Pd were not efficiently photoexcited (due to its nuclear level structure), we would not obtain prompt and significant γ-ray emission by Pd-LEPF. However, short-lived γ-rays from channels (7), (9), (21), (24) of Pd-104 and -106 should be observed experimentally. The existence of γ-rays observed during CF experiments should be further researched to resolve this contradiction.

The model of channel-dependent fission barriers can be applied to elements of $A > 90$ which can have positive Q values for scissions. Since Ohmori *et al.*[3] have reported transmuted elements in their electrolysis experiment using a ^{197}Au cathode, we are proceeding with the analysis of LEPF for Au. Calculated data of E_f values for ^{197}Au LEPF are shown in Fig. 7. We immediately see the

Table VI. List of isotope yield data for LB2 of Pd LEPF.

FP		Pd-102 (1.02%)		Pd-104 (11.14%)		Pd-105 (22.33%)		Pd-106 (27.33%)		Pd-108 (26.46%)		Pd-110 (11.72%)		Pd-nat. (%)		Element (%)	
$_{6}$C	-12	1	(1)											1	(0.02)	1	(0.02)
$_{8}$O	-16	1	(1)	1	(11)	1	(22)	1	(27)					62	(1.07)	84	(1.45)
	-17					1	(22)							22	(0.38)		
$_{10}$Ne	-22									1	(27)			27	(0.46)	26	(0.46)
$_{12}$Mg	-26							1	(27)	1	(27)			54	(0.93)	54	(0.93)
$_{14}$Si	-28	1	(1)									1	(12)	13	(0.22)		
	-29					1	(22)							22	(0.38)	223	(3.85)
	-30	1	(1)	1	(11)	1	(22)	1	(27)	1	(27)			88	(1.52)		
	-32*	1	(1)	1	(11)	1	(22)	1	(27)	1	(27)	1	(12)	100	(1.72)		
$_{15}$P	-31					1	(22)							22	(0.38)	23	(0.40)
	-33*	1	(1)											1	(0.02)		
$_{16}$S	-34	1	(1)	1	(11)	1	(22)	1	(27)					62	(1.07)		
	-35*	1	(1)			1	(22)							23	(0.40)	185	(3.19)
	-36	1	(1)	1	(11)	1	(22)	1	(27)	1	(27)	1	(12)	100	(1.72)		
$_{17}$Cl	-37	1	(1)	1	(11)	2	(45)							57	(0.98)	56	(0.98)
$_{18}$Ar	-38	1	(1)	1	(11)	2	(45)							57	(0.98)		
	-39*	1	(1)			1	(22)							23	(0.40)	268	(4.63)
	-40	1	(1)	1	(11)	1	(22)	1	(27)	1	(27)			88	(1.52)		
	-42*	1	(1)	1	(11)	1	(22)	1	(27)	1	(27)	1	(12)	100	(1.72)		
$_{19}$K	-41	2	(2)	1	(11)	1	(22)							36	(0.61)	36	(0.61)
$_{20}$Ca	-42	1	(1)											1	(0.02)		
	-43	2	(2)	1	(11)	2	(45)							58	(1.00)		
	-44	1	(1)	1	(11)	2	(45)	2	(55)	1	(27)	1	(12)	150	(2.58)	520	(8.96)
	-45*	1	(1)	1	(11)	2	(45)	2	(55)					111	(1.92)		
	-46	1	(1)	1	(11)	1	(22)	1	(27)	1	(27)	1	(12)	100	(1.72)		
	-48	1	(1)	1	(11)	1	(22)	1	(27)	1	(27)	1	(12)	100	(1.72)		
$_{21}$Sc	-45	1	(1)											1	(0.02)	2	(0.04)
	-46*	1	(1)											1	(0.02)		
$_{22}$Ti	-46	1	(1)											1	(0.02)		
	-47	3	(3)	2	(22)	2	(45)	1	(27)	1	(27)	2	(24)	147	(2.54)		
	-48	2	(2)	2	(22)	2	(45)	2	(55)					124	(2.13)	774	(13.35)
	-49	2	(2)	2	(22)	3	(67)	3	(82)	2	(53)	2	(24)	250	(4.30)		
	-50	1	(1)	2	(22)	2	(45)	3	(82)	3	(80)	2	(24)	253	(4.36)		
$_{23}$V	-49*	1	(1)											1	(0.02)		
	-50*	1	(1)											1	(0.02)	241	(4.15)
	-51	3	(3)	2	(22)	3	(67)	3	(82)	2	(53)	1	(12)	239	(4.12)		
$_{24}$Cr	-50	1	(1)											1	(0.02)		
	-51*	1	(1)											1	(0.02)		
	-52	3	(3)	4	(44)	3	(67)	3	(82)	1	(27)	1	(12)	235	(4.05)	758	(13.07)
	-53	2	(2)	2	(22)	3	(67)	4	(109)	2	(53)	1	(12)	265	(4.57)		
	-54	1	(1)	1	(11)	2	(45)	3	(82)	4	(106)	1	(12)	256	(4.42)		

*radio isotope.

two-peaked structure of mass distribution in the LB band, which clearly predicts the two-peaked mass distribution of fission fragments. General two-peaked mass distributions of FPs for high mass ($A > 180$) elements including U and Pu can be explained by this method based on the model of scission-channel-dependent fission barriers.

3.3 Mass distribution of FPs

Isotopic FP yield data of Pd isotope LEPF were obtained for LB1 (94 SCF channels) and LB2 (152 SCF channels) of the lowest band of selective fission channels. Results for LB2 are tabulated in Tables VI and VII. Radioactive isotopes produced are indicated by asterisks. In the tables, the numbers of fission events are given for each Pd isotope. The numbers of weighted events with the natural abundance data of Pd isotopes are given in parentheses. By summing up the numbers of weighted events, the relative isotopic yield data for natural Pd were reduced to the relative event-number and percent yields in parenthesis. By summing up the yield data for isotopes with the same Z numbers, we obtained the yield

Table VII. List of isotope yield data for LB2 of Pd LEPF.

FP		Pd-102 (1.02%)		Pd-104 (11.14%)		Pd-105 (22.33%)		Pd-106 (27.33%)		Pd-108 (26.46%)		Pd-110 (11.72%)		Pd-nat. (%)		Element (%)	
$_{25}$Mn	-53*	1	(1)											1	(0.02)		
	-54*	1	(1)	1	(11)	1	(22)							34	(0.59)	263	(4.53)
	-55	2	(2)	2	(22)	2	(45)	3	(82)	2	(53)	2	(24)	227	(3.92)		
$_{26}$Fe	-54	1	(1)											1	(0.02)		
	-55*	1	(1)											1	(0.02)		
	-56	3	(3)	3	(33)	3	(67)	3	(82)	1	(27)	1	(12)	224	(3.86)		
	-57	2	(2)	2	(22)	3	(67)	3	(82)	2	(53)	1	(12)	238	(4.10)	932	(16.06)
	-58	1	(1)	1	(11)	2	(45)	3	(82)	3	(80)	1	(12)	230	(3.96)		
	-59*	1	(1)	1	(11)	1	(22)	1	(27)	2	(53)	1	(12)	126	(2.18)		
	-60*	1	(1)	1	(11)	1	(22)	1	(27)	1	(27)	2	(24)	112	(1.93)		
$_{27}$Co	-54	1	(1)											1	(0.02)	23	(0.40)
	-60*					1	(22)							22	(0.38)		
$_{28}$Ni	-60	1	(1)											1	(0.02)	23	(0.40)
	-61	2	(2)	1	(11)	2	(45)	2	(55)	1	(27)	2	(24)	162	(2.80)		
	-62	1	(1)	1	(11)	2	(45)	2	(55)	1	(27)	1	(12)	150	(2.58)	471	(8.12)
	-63*	1	(1)	1	(11)	1	(22)					2	(24)	58	(1.00)		
	-64	1	(1)	1	(11)	1	(22)	1	(27)	1	(27)	1	(12)	100	(1.72)		
$_{29}$Cu	-65	1	(1)			1	(22)							23	(0.40)	23	(0.40)
$_{30}$Zn	-66	1	(1)	1	(11)	1	(22)	1	(27)	1	(27)	1	(12)	100	(1.72)		
	-67	1	(1)	1	(11)	2	(45)							57	(0.98)	313	(5.39)
	-68	1	(1)	1	(11)	2	(45)			1	(27)	1	(12)	95	(1.64)		
	-70			1	(11)	1	(22)	1	(27)					61	(1.05)		
$_{31}$Ga	-69	1	(1)			1	(22)							23	(0.40)	46	(0.79)
	-71					1	(22)							22	(0.38)		
$_{32}$Ge	-70	1	(1)											1	(0.02)		
	-72	1	(1)	1	(11)			1	(27)	1	(27)			66	(1.14)		
	-73					1	(22)							22	(0.38)	239	(4.12)
	-74	1	(1)	1	(11)	1	(22)	1	(27)			1	(12)	74	(1.27)		
	-76					1	(22)	1	(27)	1	(27)			76	(1.31)		
$_{33}$As	-75					1	(22)							22	(0.38)	22	(0.38)
$_{34}$Se	-78									1	(27)	1	12	38	(0.66)		
	-80							1	(27)					27	(0.47)	104	(1.79)
	-82									1	(27)	1	(12)	38	(0.66)		
$_{36}$Kr	-86									1	(27)			26	(0.46)	26	(0.46)
$_{38}$Sr	-86	1	(1)											1	(0.02)		
	-88			1	(11)	1	(22)							33	(0.58)	84	(1.45)
	-89*					1	(22)							22	(0.38)		
	-90*							1	(27)					27	(0.47)		
$_{40}$Zr	-90	1	(1)											1	(0.02)	1	(0.02)

*radio isotope.

data of FP elements. By summing up the yield data for the same mass values, we also obtained the massdistribution data which is shown in Figs. 8 and 9, respectively, for LB1 and LB2, and compared with the experimental EPMA and SIMS data reported by Mizuno *et al*.[1)]

Approximately symmetrical mass distributions around $A = 50$ are obtained for LB1 and LB2. We understand the data spread in both the lower and higher mass regions when we deepen the photoexcitation from LB1 to LB2. FPs are stable isotopes except for those of ^{35}S, ^{42}Ar, ^{45}Ca, ^{50}V, ^{51}Cr, ^{53}Mn, ^{59}Fe, ^{60}Fe, ^{63}Ni, ^{89}Sr and ^{90}Sr for LB1, and ^{32}Si, ^{35}P, ^{39}Ar, ^{46}Sc, ^{49}V, ^{54}Mn, ^{55}Fe and ^{60}Co for LB2. The contribution of ^{35}P, ^{39}Ar, ^{46}Sc, ^{49}V, ^{55}Fe and ^{60}Co is small. ^{42}Ar has a rather large yield, but ^{42}Ar (32.9 y) decays with pure (100%) β^- ($Q_\beta = 600$ keV) emission to ^{42}K (stable) and is difficult to detect from outside the CF cell.

The mass distribution curve shows major peaks at around $A = 49$, 52 and 56 which correspond to ^{49}Ti, ^{52}Cr and ^{56}Fe. Other significant peaks are seen at ^{16}O, ^{36}S, ^{40}Ar, ^{70}Zn for LB1. We can state that the overall qualitative agreement with Mizuno *et al*.'s[1)] experiment is good.

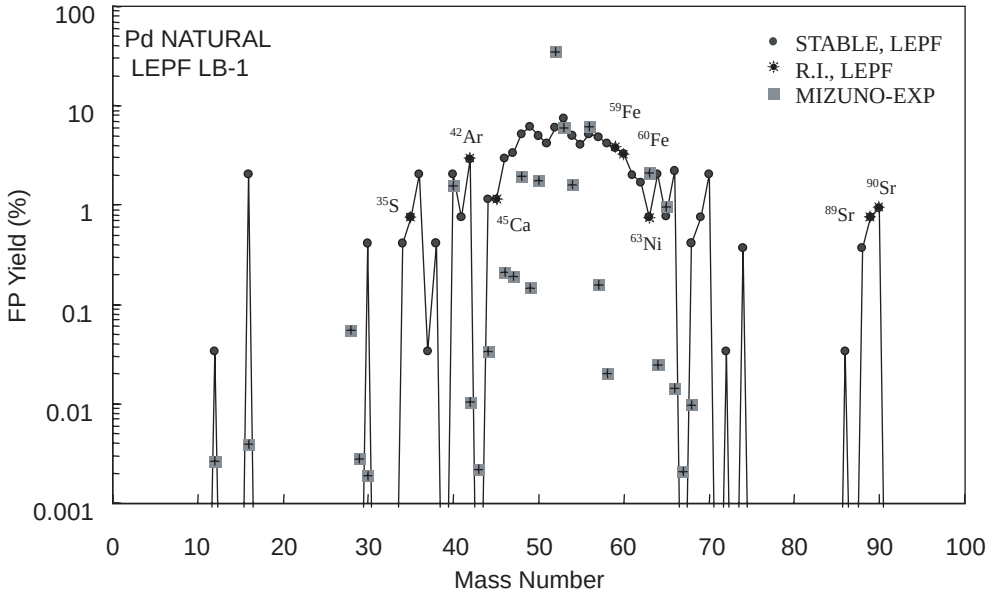

Fig. 8. FP mass distribution in LEPF/LB1 model for Pd, compared with experimental results reported by Mizuno *et al.*[1)]

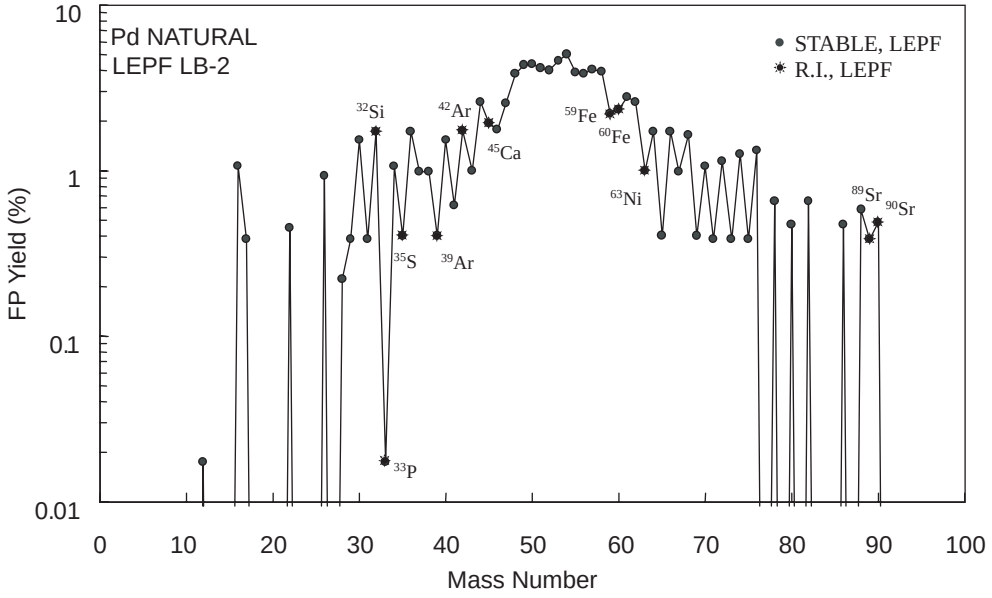

Fig. 9. FP mass distribution in LEPF/LB2 model for Pd.

3.4 Z-distribution

Theoretically obtained Z-distribution data are plotted in Figs. 10 and 11 for LB1 and LB2, respectively. Experimental EDX data obtained by Mizuno *et al.*[1)] are plotted in the same graphs for comparison. As shown in Fig. 11 and Tables VI and VII, stable FP elements are distributed from $Z = 8$ (O) to $Z = 40$ (Zr). Fe, Ti and Cr are the most dominant products, followed by Ca, Ni, Zn, Ar, Mn, V, Ge, Si, S, Se, O, Sr, Cl, Mg, Ga, K, Ne, Kr, P, Co, Cu, As, Sc, C and Zr, in the order of yield strength. The pattern of Mizuno *et al.*'s[1)] experimental data is in agreement with the LB1 data for the overall Z-region, except for the Ar and Ni peaks. By increasing selective channel fission (SCF) channels from LB1 to LB2, element yields at the right and left wings increase. However, the main part of $Z = 14$ to 30 shows a similar distribution to that of LB1 and hence maintains agreement with Mizuno *et al.*'s[1)] data.

Yield strength draws periodical peaks at even Z-values. The effect of the nuclear shell structure, particularly for α-clustered nuclei such as ^{16}O, ^{20}Ne, ^{28}Si, ^{48}Ca, ^{48}Ti, ^{52}Cr and ^{56}Fe, for selective scission channels with low fission barriers can explain this even Z-effect.

3.5 Isotopic ratios

Detailed data for isotope production are given in Tables VI and VII. For the purpose of comparison with the experimental data obtained by Mizuno *et al.*[1)] and Iwamura *et al.*,[4)] normalized (100% for each element) data for even Z elements are given in Table VIII, where natural isotopic ratios are given for comparison. FP isotopes of Pd-LEPF are markedly different from those of natural elements, as seen in Tables VI, VII and VIII.

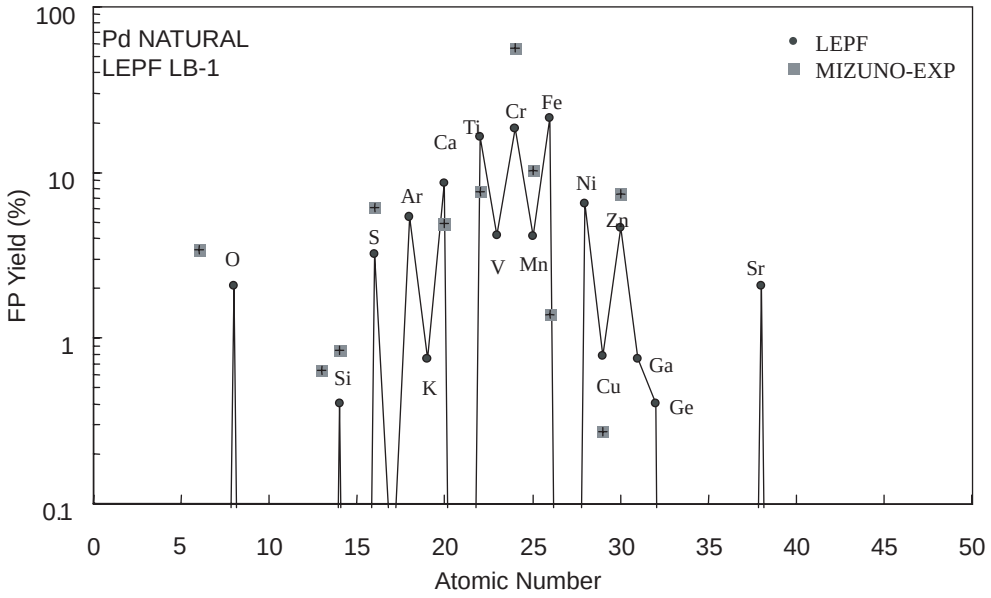

Fig. 10. *Z*-distribution in LEPF/LB1 model for Pd, compared with experimental data reported by Mizuno *et al*.[1)]

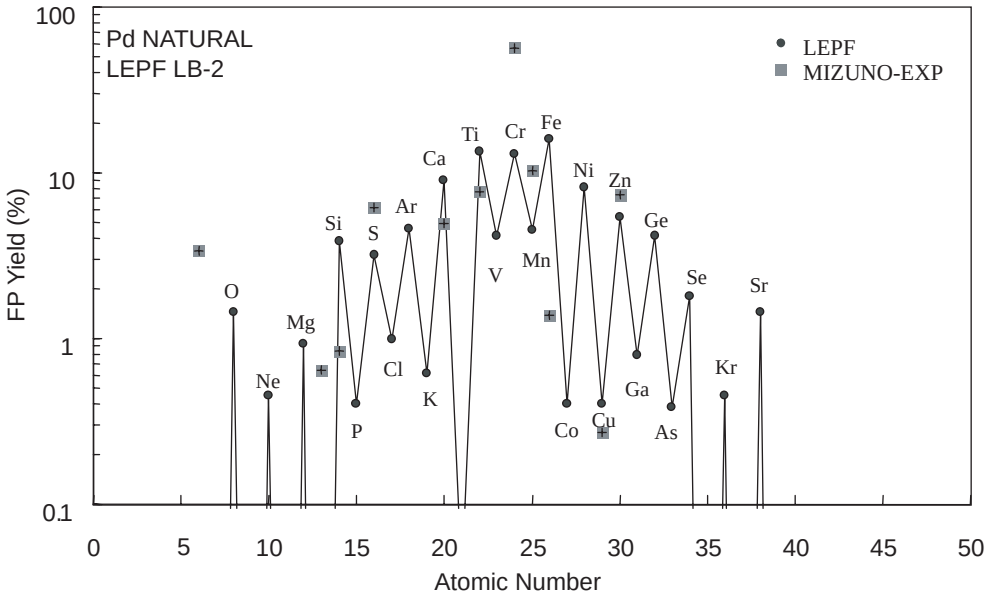

Fig. 11. *Z*-distribution in LEPF/LB2 model for Pd, compared with experimental data reported by Mizuno *et al*.[1)]

In the case of Mg, the LEPF theory predicts the production of ^{26}Mg only, compared with 78.99/10.0/11.01 for ^{24}Mg/^{25}Mg/^{26}Mg with natural Mg abundance.

In the case of Si, more ^{30}Si will be produced than ^{28}Si. For S, ^{34}S and ^{36}S are more abundant products compared with 95.02/0.75/4.21/0.02 for ^{32}S/^{33}S/^{34}S/^{36}S of the natural element.

In the case of Cl, ^{37}Cl is selectively produced, which differs from the natural ratio of 75.77/24.23 for ^{35}Cl/^{37}Cl. In the case of K, ^{41}K is also produced selectively.

In the case of Ca, the ^{40}Ca/^{42}Ca/^{43}Ca/^{44}Ca/^{46}Ca/^{48}Ca ratio by LEPF/LB2 is 0/0.2/14.2/36.6/24.5/24.5, compared with the natural isotopic ratio of 96.94/0.647/0.135/2.086/0.004/0.187. In particular, the dominant production of ^{48}Ca in the top ten channels (see Table IV) is interesting due to the double magic nuclear shell structure of ^{48}Ca. The dominant production of ^{48}Ca might be superimposed the ^{48}Ti peak in the secondary ionization mass spectrometry (SIMS) analysis experiment.

In the case of Ti, the ^{46}Ti/^{47}Ti/^{48}Ti/^{49}Ti/^{50}Ti ratio by LEPF/LB2 is 0.1/19.0/16.0/32.2/32.6, compared with the natural data of 8.25/7.44/73.72/5.41/5.18. We observe a marked enhancement for ^{49}Ti and ^{50}Ti. If we observe a dominant peak of ^{50}Ti, we must be careful not to confuse it with ^{50}Cr peak in SIMS analysis.

In the case of Cr, the ^{50}Cr/^{52}Cr/^{53}Cr/^{54}Cr ratio by LEPF/LB2 is 0.1/31.0/35.0/33.8, which is very different from the natural ratio of 4.34/83.79/9.5/2.36.

In the case of Fe, the ^{54}Fe/^{56}Fe/^{57}Fe/^{58}Fe ratio by LEPF/LB2 is 0.1/32.3/34.4/33.2, which is very different from the natural ratio of 5.84/91.75/2.12/0.28.

In the case of Ni, Zn, Ge, Se, Sr and Zr, we observe similar

Table VIII. Comparison of isotopic ratios between natural, Pd-LEPF/LB1 and experiments, for even-Z elements.

Isotope		Natural (%)	LEPF/LB1 (%)		Exp (%)	(Mizuno *et al.*[1]) (%)
Ca	-40	96.94	0.0		(45)	
	-42	0.647	0.0		0.6	
	-43	0.135	0.0		1.7	
	-44	2.086	17.6		41.1	
	-45		17.6			
	-46	0.004	29.4		35	
	-48	0.187	35.3		25	
Ti	-46	8.25	0.0		15	
	-47	7.44	20.7		9	
	-48	73.72	13.8		10	
	-49	5.41	37.9		4	
	-50	5.18	27.6		62	
Cr	-50	4.345	0.0		3	
	-51		3.1			
	-52	83.789	37.5		68	
	-53	9.501	34.4		16	
	-54	2.365	25.0		13	
Fe	-54	5.845	2.8	(3.3)[a]	13	
	-56	91.754	25.0	(30.0)[a]	64	45[4]
	-57	2.119	22.2	(26.7)[a]	16	41[4]
	-58	0.282	19.4	(23.3)[a]	7	14[4]
	-59		13.9	(16.7)[a]		
Ni	-58	68.077	0.0			
	-60	26.223	0.0			
	-61	1.140	25.0			
	-62	3.634	33.3			
	-63		8.3			
	-64	0.926	33.3			
Zn	-64	48.6	0.0		38	
	-66	27.9	44.4		18	
	-67	4.1	0.0		0	
	-68	18.8	22.2		12	
	-70	0.6	33.3		33	
Ge	-70	21.23	0.0			
	-72	27.66	50.0			
	-73	7.73	0.0			
	-74	35.94	50.0			
	-76	7.44	0.0			

a) exclude Fe-60.

trends. In the case of Cu we observe selective ^{65}Cu production by LEPF.

Thus the observation of isotopic ratios for foreign deposit elements during CF experiments is of key interest for comparison with the LEPF theory of stable isotope production by photofission.

In Table VIII, we compare the isotopic ratios obtained by the LEPF with LB1 to those of experimentally deduced values obtained by Mizuno *et al.*[1] and Iwamura *et al.*[4] For Ti, Cr, and Fe and Zn, anomalous data obtained through experiments can be qualitatively (and quantitatively, in order) explained. SIMS data should be carefully reanalyzed consistency with Z (atomic number)-distribution data determined by EDX, WDX, EPS and other methods.

4. Summary and Conclusions

Using crude assumptions of 10–50 keV high peak flux photon sources as random short bursts in dynamic PdD_x lattice, multiphoton E1 absorption, collective nucleus deformation and selective channel fission, the possibility of obtaining radiationless fission products with nonnatural isotopic ratios was investigated and confirmed by conservative model analyses. As a result, we draw the following conclusions:

1) Major production of nonradioactive elements around $Z = 24$ can be predicted by the theory of low energy photo-fission via selective channel fission (LEPF/SCF), for ^{102}Pd, ^{104}Pd, ^{105}Pd and ^{106}Pd, with small contributions by ^{108}Pd and ^{110}Pd.
2) The dominant stable FP elements are Fe, Ti, Cr, Ca, Ni and Zn, and other elements such as Ar, Mn, V, Ge, Si, S, Se, O, Co, Sr, Cl, Mg, Ga, K and Ne follow. Production of even-Z elements is enhanced.
3) Isotopic ratios of FPs generated by LEPF/SCF are very different from natural isotopic ratios for major FP elements, namely, Ca, Ti, Cr and Fe and others such as Mg, Si and Cu.

We have found consistent agreement between LEPF/SCF theory and several CF experiments regarding mass distribution, Z-distribution and nonnatural isotopic ratios. These finding strongly support the mechanism of LEPF in metal-hydride systems under electrochemical conditions. However, the present LEPF model should be further studied with regard to the following issues:

4) The understanding of the photon source and the pumping-up scenario in multiphoton absorption and nuclear collective excitation process is based on crude assumptions in the present model, and should be further studied for achieving of the condition of $E_x \sim E_r$.
5) The role of $PdD_x(H_x)$ dynamics (plasmon), in other words, the coupling of QED photons and nuclear excitation, is yet to be clarified.
6) Other competing reactions, for example, the quenching of collectively excited nuclear states by emitting gamma-rays and the possibility of prompt γ-ray emissions from fission fragments of LEPF, are yet to be studied.

In relation to items 4) through, 6) we consider that the collective nuclear excitation and deformation may selectively open LEPF/SCF. It is possible that the linkage with the coherent multibody fusion[6] of deuterons is responsible for the existence of strong peak flux bursts of $\sim$50 keV QED photons.

7) Ni and Ti have no exothermic fissions due to largely negative Q values (-5 to -40 MeV).
8) LEPF/SCF is possible in principle, if nuclear excitation ($E_x \sim E_r$) is realized by some external means (for example, photon beam), for $A > 90$.
9) Experiments such as those conducted using the short-pulse X-ray laser, plasma discharge and glow-discharge-state electrolysis may be of considerable interest in this respect.
10) Apart from the explanation of CF results, LEPF/SCF is a new idea which may be considered for the incineration (transmutation) of high radio-active nuclear waste and clean power generation from heavy elements with

positive Q values of scissions ($Q > 100\,\mathrm{MeV}$; for $A > 180$), if the phenomenon is substantiated by pure irradiation experiments using ns-fs short pulse X-ray and fs-peta-watt lasers. We are awaiting the implementation of such pure physics experiments.

Acknowledgments

The authors extend their appreciation to Dr. Y. Iwamura (Mitsubishi Heavy Industry) and Professor G. Miley (University of Illinois) for their valuable comments on this work.

1) T. Mizuno, T. Ohmori, K. Kurokawa, T. Akimoto, M. Kitaichi, K. Inoda, K. Azumi, S. Shimokawa and M. Enyo: Denki Kagaku **64** (1996) 1160 [in Japanese].
2) G. Miley and J. Patterson: J. New Energy **1** (1996) No. 3, 5.
3) T. Ohmori, T. Mizuno, Y. Nodasaka and M. Enyo: Fusion Technol. **33** (1998) 367.
4) Y. Iwamura, T. Itoh, N. Gotoh and I. Toyoda: Fusion Technol. **33** (1998) 476.
5) H. Kozima: *Discovery of the Cold Fusion Phenomenon* (Ohtake, Tokyo, 1998).
6) A. Takahashi, T. Iida, H. Miyamaru and M. Fukuhara: Fusion Technol. **27** (1995) 71.
7) A. Takahashi, K. Maruta, K. Ochiai, H. Miyamaru and T. Iida: Fusion Technol. **34** (1998) 256.
8) A. Takahashi, K. Maruta, K. Ochiai and H. Miyamaru: Phys. Lett. A **255** (1999) 89.
9) H. Fukuoka, T. Ikegawa, K. Kobayashi and A. Takahashi: Proc. 6th Int. Conf. Cold Fusion, Toya, 1996, p. 425.
10) G. Preparata: Proc. 2nd Annu. Conf. Cold Fusion, Como, 1990, p. 453.
11) C. L. Lederer and U. S. Shireley: *Table of Isotopes* (John Wiley & Sons, New York, 1990) 8th ed.
12) K. Sugimoto and M. Muraoka: *Genshikaku Butsurigaku* (Nuclear Physics) (Kyoritsu, Tokyo, 1988) [in Japanese].
13) S. Glasstone and M. C. Edlund: *The Elements of Nuclear Reactor Theory* (D. Van Nostrand, New York, 1952).
14) K. Yagi: *Genshikaku Butsurigaku* (Nuclear Physics) (Asakura, Tokyo, 1989) [in Japanese].
15) *Reactor Physics Constants ANL-5800* (United States Atomic Energy Commission, Washington D.C., 1963) 2nd ed., p. 6.
16) M. Ohta, M. Matsunaka and A. Takahashi: Jpn. J. Appl. Phys. **40** (2001) 7047.